Green Chemistry

Alkanolamines as Dual Functional Solvents for Biomass Deconstruction and Bioenergy Production

Journal:	*Green Chemistry*
Manuscript ID	GC-ART-07-2021-002667.R1
Article Type:	Paper
Date Submitted by the Author:	20-Sep-2021

Complete List of Authors:	Achinivu, Ezinne; Joint BioEnergy Institute, Deconstruction Frank, Skye; University of California Davis, ; Baral, Nawa Raj; Lawrence Berkeley National Laboratory, LEAD; Das, Lalitendu; Joint BioEnergy Institute; Sandia National Laboratories, Deparment of Biomass Science and Conversion Technology Mohan, Mood; Joint BioEnergy Institute, Deconstruction; Sandia National Laboratories, Department of Biomass Science and Conversion Technology Otoupal, Peter; Lawrence Berkeley National Laboratory, Joint BioEnergy Institute; Sandia National Laboratories California, Biomass Science and Conversion Technology Shabir, Emara; Ernest Orlando Lawrence Berkeley National Laboratory Utan, Sean; Ernest Orlando Lawrence Berkeley National Laboratory Scown, Corinne; Lawrence Berkeley National Laboratory, Energy Analysis and Environmental Impacts Division; Joint BioEnergy Institute, LEAD Simmons, Blake; E O Lawrence Berkeley National Laboratory, Biological Systems and Engineering Gladden, John; Joint BioEnergy Institute, Deconstruction

Alkanolamines as Dual Functional Solvents for Biomass Deconstruction and Bioenergy Production

Ezinne C. Achinivu,[a,b] Skye Frank,[a,c] Nawa Raj Baral,[a,c] Lalitendu Das,[a,b] Mood Mohan,[a,b] Peter Otoupal,[a,b] Emara Shabir,[a,b] Sean Utan,[a,b] Corinne D. Scown,[a,c] Blake A. Simmons,[a,c] John Gladden*[a,b]

[a]Joint BioEnergy Institute, Lawrence Berkeley National Laboratory, 5885 Hollis St, Emeryville, CA 94608, USA.

[b]Sandia National Laboratories, 7011 East Ave, Livermore, CA 94551, USA.

[c]Biological Systems and Engineering Division, Lawrence Berkeley National Laboratory, Berkeley, CA 94720, USA.

*Corresponding Author

Email: jmgladden@lbl.gov; jmgladd@sandia.gov (J. M. Gladden)

ABSTRACT

This work demonstrates the feasibility of applying dual functional solvents called alkanolamines towards the conversion of biomass into biofuels. Alkanolamines have the potential to serve as effective pretreatment solvents that promote a low energy intensity, process intensification, and downstream conversion via a cost-effective route. Several key factors were considered to effectively integrate the pretreatment technology into a biorefinery, including solvent screening (both experimentally and computationally), feedstock screening (capturing the effectiveness on softwood, hardwood, and grasses), fractionation of lignocellulose components (lignin removal), bioconversion efficacy, and a sustainability impact assessment. After a thorough and systematic optimization, the following conditions emerged for optimal process economics (i.e., shortest time, lowest temperature, and highest solid loading): pretreatment of sorghum biomass via ethanolamine (25% solvent in water) with temperature 100 °C, time 1h and solid loading 40%. These conditions generated yields of 90% glucose, 76% xylose, 59% lignin removal, and 73% solid recovery. The pretreated biomass and recovered lignin were studied using PXRD/TGA/FTIR/NMR analyses, revealing that the morphology and crystallinity of biomass does not change after pretreatment, and recovered lignin is dominated by guaiacyl groups, which are suitable for lignin valorization. Subsequently the process was consolidated and scaled up (40X) to generate >99% sugar yields followed by a test of bioconversion using the omnivorous host *R. toruloides*, which converted >97% C5, C6 and phenolic into the biofuel precursor bisabolene at a titer of 1155 mg/L. The TEA revealed that the cost of biomass deconstruction was severely reduced (up to 50%) compared to similar pretreatment methods, including ethanolamine acetate and cholinium lysinate, evaluated under the same modeling assumptions. This study has demonstrated the effectiveness and robustness of alkanolamines towards biomass processing and presents a new solvent group to be considered for biomass pretreatment within a commercial biorefinery for the deconstruction of lignocellulosic biomass.

INTRODUCTION

The transformation of waste lignocellulosic biomass to commercially viable bioproducts (biofuels, biochemicals etc.) in a biorefinery is a promising strategy with the potential to substantially reduce dependence on petroleum based resources and mitigate climate change.[1] To develop a competitive biorefinery, each step/unit operation (including pretreatment, saccharification, bioconversion and separation/recovery) must be optimized to derive the greatest value and net environmental benefit from the biomass feedstock.[2] Biomass pretreatment remains both a challenge and an essential step representing up to 20% of the cost in biofuel production,[3] and its effectiveness can significantly influence the efficacy of downstream processes. Largely owing to the recalcitrant nature of the raw biomass, pretreatment is necessary to effectively deconstruct the biomass, which is accomplished primarily by lignin removal, liberating and exposing the plant polysaccharides for efficient enzymatic digestion.[4] Defining the best pretreatment method can be difficult, however, each strategy must be carefully studied, optimized and integrated with sustainability impact analyses to constructively provide recommendations for a path forward. A widely accepted approach to enable economic sustainability is to reduce the pretreatment cost and overall biorefinery cost or increase the revenue from lignocellulosic biomass by maximizing the utilization of the feedstock as well as its derivatives.[5,6] This is achieved by developing effective fractionation methods that enable downstream processing while utilizing process optimization and integration methods to achieve these goals with the least amount of resources, energy and environmental impact.

Many different pretreatment approaches have been investigated and the most effective approaches often rely on high levels of lignin extraction from the biomass. These strategies include four chemical industrial processes that are noteworthy for lignin removal: sulfite, kraft, soda and organosolv.[7,8] Amongst these, the organosolv fractionation process has been widely accepted as one of the most promising strategies for biomass fractionation due to its comparatively low environmental impact, high delignification efficiency, and the diversity of products that are released.[5,9,10] In this pretreatment method, organic solvents are utilized as the primary constituent to facilitate biomass fractionation either by lignin and/or hemicellulose removal.[11,12] Alkanolamines are dual functional solvents that can serve as both Brønsted base (proton/hydrogen ion acceptor) and hydrogen bond donor/acceptor for a variety of chemical reactions. This unique

combination presents a highly potent lignin solvent that is associated with high delignification efficiency and pulp yield.[13] Nevertheless, due to inefficient process optimization, integration, and separation methods, the efficacy of downstream processes (bioconversion and lignin utilization) have been limited, and these pretreatment methods have not been fully evaluated for their sustainability within a biorefinery. A survey of the literature reveals that these solvents have been historically used in conjunction with other chemical species during pretreatment (such as chemical pulping solutions, liquids salts called ionic liquids (ILs), and deep eutectic solvents (DESs). In each of these scenarios, alkanolamines have been demonstrated to have a utility in facilitating lignin removal and subsequently improving sugar release from the biomass. Alkanolamines have been applied in combination with organic acids to prepare protic ionic liquids such as ethanolamine (or 2 amino 1 ethanol) acetate for biomass pretreatment, which resulted in improved rates of lignin removal with increased glucose yields.[14–17] Similar results were also observed with ethanolamine based DESs where choline chloride: ethanolamine DESs were employed to remove 71% lignin and reserve 94% cellulose, while also improving the enzymatic hydrolysis of the residue, i.e., 90% cellulose and 62% xylan conversion.[18] Paper pulps produced using ethanolamine (in combination with soda) as a solvent demonstrate favorable properties such as viscosity, drain index, and low kappa values.[19–21] Highest rates of delignification and glucan conversion are exhibited when the pulping methods were applied to grasses, such as wheat straw, as opposed to hardwoods.[22] Compared to pulps created by conventional glycol methods, ethanolamine based pulps exhibit better drainage index, viscosity, and burst across various studies.[20]

Despite these impressive results, there is evidence to suggest that alkanolamines alone might promote the high deconstruction efficiency that is needed for effective biomass pretreatment.[13] The use of alkanolamines as the sole solvent will enable the development of a simplistic and effective pretreatment process that will be more cost effective through eliminating the need for relatively higher cost solvents, such as certain ionic liquids. Alkanolamine-based mixed solvents (like ionic liquids) are often characterized by higher viscosities,[23] which limits mass transfer/diffusivity and solvation capacity,[24] therefore, requiring longer reaction times, higher temperature and lower solid loading—all factors that can increase operational costs. Sun *et al.* observed higher lignin removal as both temperature and time was increased to 160 °C, 3h using ethanolamine acetate. Pretreatment solvents also need to be biocompatible and effective in the presence of water to enable process consolidation and downstream processes[25] The use of

alkanolamines as an individual solvent may overcome some of these issues, so there is an opportunity to design a low temperature process with minimal energy input while reducing reaction time, increasing solids loading, and maintaining biocompatibility.

The purpose of this study is to expansively study the use of alkanolamines as molecular solvents for biomass pretreatment to promote lignin and/or hemicellulose removal and increase polysaccharide digestibility. This study begins with a screen of several alkanolamines (computational and experimental) to identify a single high-performing solvent. Next, the down selected solvent is tested on several different types of biomasses, followed by rigorous process optimization and consolidation to optimize pretreatment conditions, and a final scale up demonstration. The process was then vetted for effective downstream bioconversion of the biomass hydrolysate and a techno economic analysis of the final process economics/feasibility was conducted.

RESULTS/DISCUSSION

PRELIMINARY SCREENING

Deconstruction of Sorghum Biomass using Different Alkanolamines

A diverse group of alkanolamines were screened for their pretreatment effectiveness. The solvents were selected by varying the chemical conformation, substituents, and the number of functional groups in the alkanolamine backbone (Figure 1 and Table S1). Pretreatment effectiveness is typically measured based on the amount of sugar released after pretreatment and enzymatic hydrolysis, as well as the lignin and/or hemicellulose extraction capacity of the solvent.

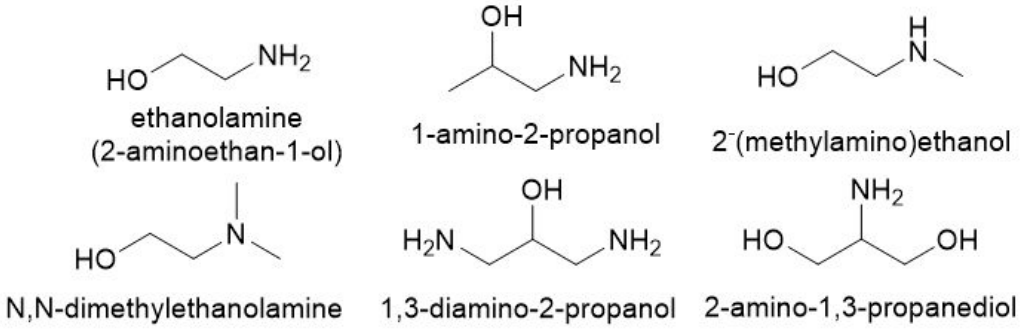

Figure 1. Chemical Structures of alkanolamines utilized in this study.

Figure 2A (and S1) lists the rates of lignin removal (hemicellulose removal) and solids recovered with respect to the pretreatment solvent employed. With the exception of biomass pretreated by N, N-dimethylethanolamine, lignin removal falls between 75-80% while solid recovery averages at 60%. In contrast, the lignin removal of N, N-dimethylethanolamine pretreated biomass falls below 20% and has the highest solid recovery of any pretreatment solvent with around 80% biomass recovered. This is expected since low lignin extraction indicates a higher solid retention in the recovered biomass. Figure 2B, displays the glucose and xylose yields resulting from the following enzymatic hydrolysis of the pretreated biomass. The data exhibits similar trends to the lignin removal where glucose yields average around 85-90% for each solvent while xylose differs between each solvent. N, N-dimethylethanolamine and 1,3-diamino-2-propanol pretreated biomass exhibited the lowest rates of hemicellulose conversion with xylose yields of approximately 35%. Additionally, N, N-dimethylethanolamine pretreated biomass yielded about 40% lower glucose yields than those of the suite of solvents. ethanolamine exhibited xylose yields around 65% while the biomass pretreated by the remaining solvents demonstrated xylose yields of 75-80%. Overall, ethanolamine, 1-amino-2-propanol and 2-(methylamino)ethanol were the most effective in terms of obtaining the highest total sugar yields.

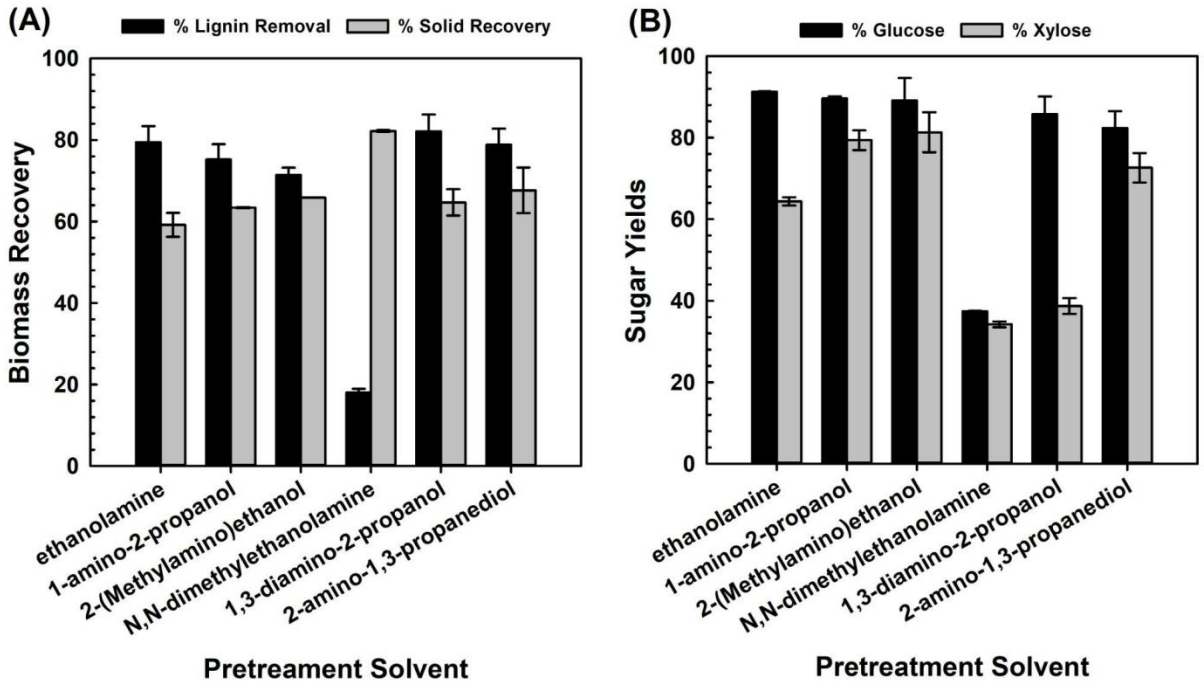

Figure 2. (A) Lignin removal, solid recovery after biomass pretreatment with alkanolamines and (B) glucose and xylose yields recovered after enzymatic hydrolysis of the sorghum recovered after pretreatment with alkanolamines.

In general, the results indicate a direct correlation between lignin removal efficiency and holocellulose digestibility (sugar release) (Figure 2). In addition, there is a direct trend associated with degree of substitution on the amine group and the lignin removal/sugar release efficiency (primary vs. secondary vs. tertiary amine). Therefore, to gain a better understanding of the observed trends for alkanolamines on biomass pretreatment and lignin removal, COSMO-RS calculations were performed to evaluate the thermodynamic properties such as excess enthalpy and activity coefficient. This will also help in understanding mechanistic reasons and driving factors that promote effective pretreatment (lignin removal and sugar release). Figure 3 reports the COSMO-RS predicted excess enthalpy (H^E) and logarithmic activity coefficients ($\ln(\Upsilon)$) between lignin and alkanolamines, as well as that of hemicellulose. Both H^E and $\ln(\Upsilon)$ are useful thermodynamic properties for measuring the difference in the strength of interactions between different species (i.e., lignin - solvents) in the mixture. The lower values (i.e., more negative) of H^E and $\ln(\Upsilon)$ results indicate stronger interactions and higher dissolving power of a solvent. From Figure 3, ethanolamine, 1-amino-2-propanol, and 1,3-diamino-2-propanol have lower H^E and $\ln(\Upsilon)$ of lignin than other alkanolamines, results that are in line with the fact that these solvents each show a higher removal capability for lignin (~75-82%). In contrast, N, N-dimethylethanolamine had H^E and $\ln(\Upsilon)$ of lignin that were predicted to be weaker, which implies that N, N-dimethylethanolamine has lower dissolution capability for lignin and was verified experimentally (~18%). These results demonstrate a direct correlation between the experimental results and the COSMO-RS predicted lignin interactions. Interestingly, a screen for hemicellulose solubility capacity also shows similar trends, which can help understand the changes in xylose yields observed experimentally (Figures 2B, 3B). When hemicellulose is dissolved during pretreatment, the resultant sugar release will be lower. In the case of 1,3-diamino-2-propanol and ethanolamine, the lower xylose release is not due to an ineffective pretreatment but due to the loss of dissolved polysaccharides during biomass recovery (biomass is water washed after pretreatment during screening). On the other hand, N, N-dimethylethanolamine has lower dissolution capability for hemicellulose and biomass was not effectively deconstructed as indicated by low lignin and hemicellulose solubility (Figure 3B).

Another noteworthy observation is that the primary and secondary amines are predicted to be better solvents for lignin removal (80% and 72%) than tertiary amine-based solvent (18%). For example, the H^E and ln(Υ) of lignin in primary (ethanolamine) and secondary (2-(methylamino) ethanol) amines are predicted to be strong lignin and hemicellulose solvents (i.e., -1.35 kJ/mol / -0.53 kJ/mol and -2.07 / -1.74, respectively), while the tertiary amine (N, N-dimethylethanolamine) H^E and ln(Υ) of lignin values are predicted to be 0.08 kJ mol^{-1} and -1.29, respectively. The lower capability for lignin dissolution of tertiary amine is due to the reduced polarity of N, N-dimethylethanolamine which leads to a weaker interaction between lignin and tertiary N, N-dimethylethanolamine (see Figure S2).

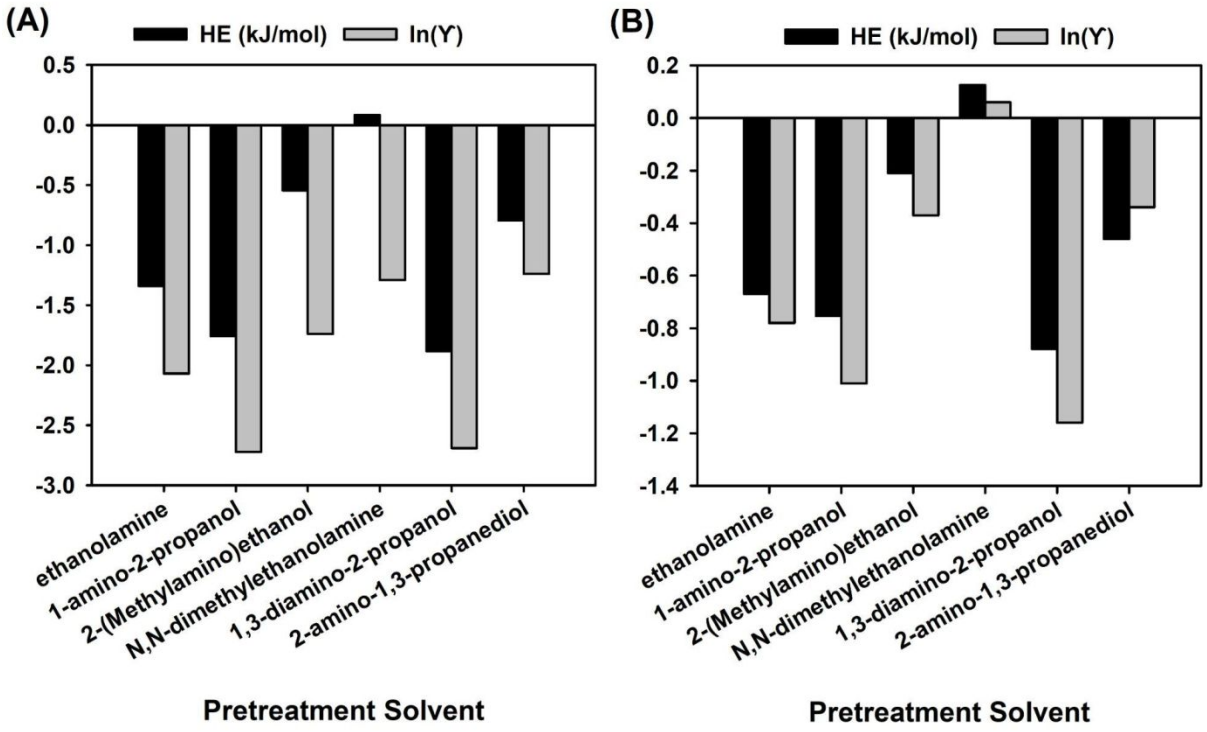

Figure 3. COSMO-RS predicted excess enthalpy and logarithmic activity coefficients of (A) hemicellulose and (B) in lignin in alkanolamines.

The most impactful observation was that an increase in the number of primary amine functional groups increased, the removal of lignin also increased (e.g., 1-amino-2-propanol (-NH_2: 75%) *vs* 1,3-diamino-2-propanol (-2(NH_2): 82%)). Additionally, increasing the hydroxyl groups (-OH) was effective at improving the lignin removal, where the removal of lignin also increased (1-amino-2-propanol (-OH: 75%) *vs* 2-amino-1,3-propanediol (-2(OH): 79%)). However, with a comparison

between 1,3-diamino-2-propanol (-2(NH_2): 82%) and 2-amino-1,3-propanediol (-2(OH): 79%), the primary amine dominated solvent (1,3-diamino-2-propanol) was found to be marginally better solvent for lignin removal than hydroxyl group dominated solvent (2-amino-1,3-propanediol). This can be further explained by measuring the sigma potential of 1,3-diamino-2-propanol and 2-amino-1,3-propanediol, which indicates that 1,3-diamino-2-propanol has a stronger affinity to interact with hydrogen bond donor groups of lignin than 2-amino-1,3-propanediol (Figure S2).

The COSMO-RS predicted quantities (H^E, ln(Υ)), along with the viscosity and the pK_a values (Figures S3), were utilized to develop a lignin solubility prediction model for alkanolamines (see below equation). The developed model shows an excellent agreement between predicted and experimental lignin removal (R^2=1 (Figure S4)) and can be applied to predict lignin solubility in new configurations of alkanolamines, as well as, to understand the factors influencing lignin solubility. The model reveals that factors such as viscosity (representing mass transfer/diffusivity) and pK_a (representing chemical reactivity/basicity) play a significant role in the function of alkanolamines toward biomass pretreatment and lignin removal (Figure S3).

$$Lignin\ sol.\ (\%) = b_0 + \left(b_1 \times exp\left(H^E\right)\right) + \left(b_2 \times ln(\gamma)\right) + \left(b_3 \times Visc\right) + \left(b_4 \times pK_a\right)$$

$$b_0 = -209.86; b_1 = -64.52; b_2 = 16.62; b_3 = 0.32; b_4 = 35.08$$

Pretreatment Effectiveness for Different Biomass Types

Following the initial solvent screen, feedstock compatibility was also surveyed to determine how effective this process is on different biomass types and to identify the optimal biomass source to be used for further process optimization. The results from the sorghum pretreatment were compared with that of pine, almond, walnut, and fir biomass types. The ability to utilize diverse biomass feedstock is an attractive feature for any pretreatment method. Developing a feedstock agnostic chemical is a robust and economical way to mass produce biomass derived biofuels. Nevertheless, it is well known that the biomass type can influence the pretreatment effectiveness.[26–28] Based on their composition, certain softwoods (pine/fir) may have higher carbohydrate content compared to hardwoods and herbaceous biomass (sorghum), therefore, making them economically attractive for process intensification (Figure S5). However, woody biomass is sometimes more intractable than herbaceous biomass, typically due to their higher lignin content, high cellulose crystallinity and the appearance of toxic extractives (like aromatic compounds,

terpenes and organic acids).[26,29–31] Therefore, to take advantage of the intrinsic value of softwoods and hardwoods, an effective fractionation of their constituents is essential.

The biomass surveyed represents the major categories of lignocellulosic biomass and will enable the testing of the robustness of this solvent for pretreatment.[29] In the previous section, ethanolamine, 1-amino-2-propanol and 2-(methylamino)ethanol were the most effective pretreatment solvents with the highest average sugar release (92%, 90%, 89% glucose respectively and 64%, 79%, 81% xylose respectively) (Figure 2B). Owing to its simple molecular structure, and the ease of access and cost,[32] ethanolamine was selected for further screening and process development. Using the same pretreatment conditions, several biomasses were screened for the ability of ethanolamine to extract lignin, followed by enzymatic saccharification to release monomeric sugars. Figure 4A displays the rates of lignin removal and solids recovered with respect to the biomass type. Pine and fir, both softwoods, had equally low rates of lignin removal at around 15-20% while about 75% of their solids were recovered following pretreatment. Hardwoods, walnut and almond had 50-55% lignin removal as well as 60% solid recovery. The grass sorghum had the highest rates of lignin removal at ~80%, with solid recovery rates equal to those of walnut and almond. Despite having 25% less lignin removal in comparison to sorghum, pretreated almond wood yielded nearly equivalent amounts of glucose yields at 98%, while sorghum biomass had glucose yields of 90% (Figure 4B). Almond and sorghum had slightly reduced xylose yields in comparison to their cellulose conversion with around 80% and 65%, respectively, while walnut, pine, and fir achieved glucose yields of about 80%, 20%, and 25%, respectively.

Regardless of obtaining relatively high glucose yields, the xylose yields of walnut were significantly lower at about 15%. The low lignin removal of pine and fir seem to correlate to their overall unfavorable sugar yields. This is in accordance with previously reported studies that reveal softwoods to be more difficult to pretreat due to higher lignin content and the presence of condensed lignin units.[26,28] In general sorghum and almond are the most favorable for biomass for pretreatment yielding an average of 91% and 98% glucose, respectively, along with 64% and 83% xylose, respectively. Despite the higher polysaccharide conversion for almonds, it is important to note that the raw biomass comprises only 22% glucan (precursor to glucose) and 11% xylan (precursor to xylose), while sorghum has 35% glucan and 21% xylan (Figure S5-6). Woody biomass like almonds have high amounts of extractives, which are not always easily valorized into

biofuel components. Therefore, for process intensification and effectiveness, this biomass type is not the most suitable for this process, and sorghum was selected for the remaining screening.

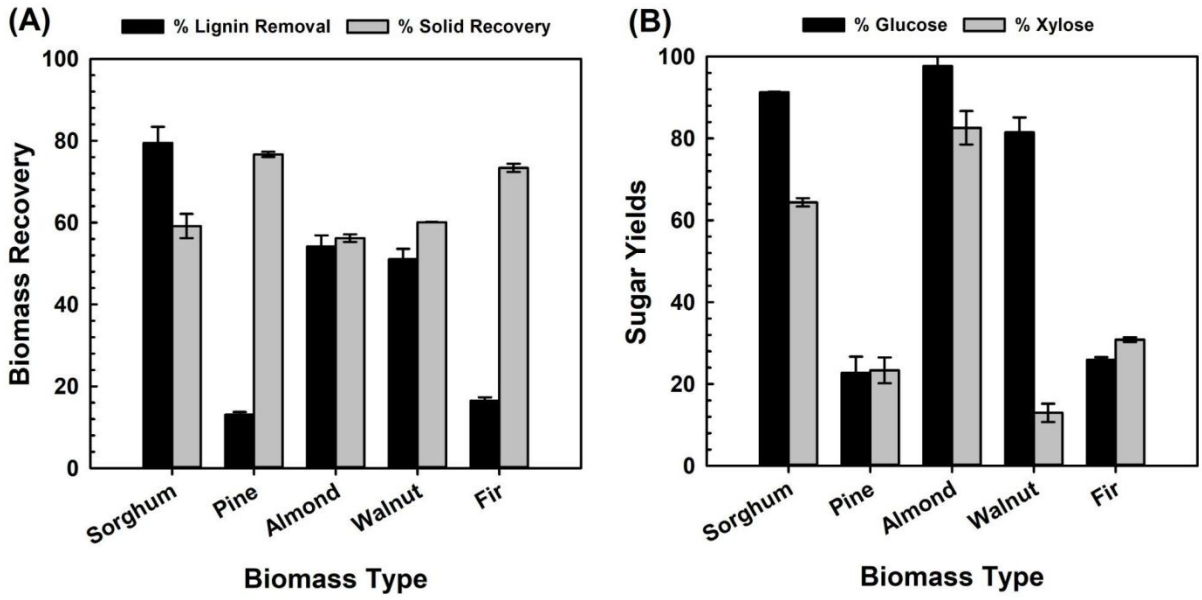

Figure 4. (A) Lignin removal, solid recovery after biomass pretreatment with ethanolamine and (B) glucose and xylose yields recovered after enzymatic hydrolysis of pretreated biomass with ethanolamine.

PROCESS DEVELOPMENT

Process Optimization using Design of Experiment (DOE)

After the solvents and biomass types were screened, an attempt was made to improve the process by varying the pretreatment conditions such as reaction time, solid loading, and reaction temperature. These factors are known to directly impact pretreatment severity,[14,28,33] and were surveyed across various levels to identify the most optimal condition in terms of lignin removal and sugar yields. Pretreatment severity was initially selected based on previous data from pretreatment studies,[14,28] however, there is a high possibility that a more optimal condition can be discovered to yield benefits in cost improvement and environmental impact. Table S2 shows the experimental and predicted results for the glucose, xylose, lignin removal, and solid recovery using central composite design (CCD). Batch optimization and model fitting for all the four-responses (above mentioned) with respect to the three independent variables (time, temperature, and solid loading) were also performed. The results illustrate that glucose yields were in the range of 72-

91%. The suggested optimum levels for glucose yield were temperature 120 ℃, time 1.8 h, and 40% solid loading, corresponding to a predicted yield of 88% at 95% confidence interval ([85, 92]). Similarly, xylose yields fell within the 63-77% range. The optimum levels for xylose yield were temperature 126 ℃, time 1h, and solid loading of 40%, corresponding to a predicted yield of 76% at 95% confidence interval ([73, 79]). In addition, lignin removed was in the range of 59-81%. The results illustrate that the optimum levels of independent variables were temperature 140 ℃, time 2.4h, and solid loading of 20%, corresponding to a predicted yield of 82% at 95% confidence interval ([78, 85]). Finally, the solid recovery from the CCD design was in the range of 52.7-72.5%. The optimum levels for solid recovery were temperature 100 ℃, time 1 h, and 40% solid loading, corresponding to a predicted yield of 70% at 95% confidence interval ([68, 72]). Further, a second-degree polynomial model was fit to the experimental data to find the optimized reaction conditions to maximize the measured responses and estimate the significance of each parameter (temperature, time, and solid loading) towards glucose yield, xylose yield, lignin removal, and solid recovery.

Solid loading: The combined (linear and interaction) effect of solid loading with reaction time and reaction temperature on glucose and xylose yield are shown in Figures 5A-I & II and 5B-I & II. Increasing the solid loading resulted in little or no change in glucose and xylose yield, with maximum yields obtained at 40% solid loading. Results from the ANOVA (Table S3) indicate that both linear and interaction effects of solid loading with reaction time and temperature were not significant ($p > 0.05$) with respect to glucose yield. Similarly, ANOVA Table S4 illustrates the linear effect of solid loading on xylose yield was significant ($p < 0.0001$), whereas interaction effect of solid loading with reaction time and temperature were not significant ($p > 0.05$). Figures 5C-I & II and S7 A&B demonstrate the combined (linear and interaction) effect of solid loading with reaction time and reaction temperature on solid recovery and lignin removal yield. Response surface plots illustrate that the changes in solid loading had significant impact on solid recovery ($p = 0.0003$) and lignin removal ($p < 0.0001$) yield. Results from the ANOVA (Table S5 and S6) indicate that within the experimental levels interaction effects of solid loading with reaction time and temperature were not significant ($p > 0.05$) for both solid recovery and lignin removal yield.

Reaction temperature: Figures 5A-II & III and 5B-II & III demonstrate the combined effect of reaction temperature with reaction time and solid loading on glucose and xylose yield. The convex

curve from the response surface plots for the reaction temperature on glucose and xylose yield indicates that maximum yield is obtained when the reaction temperature lies between 100 and 140 ℃. Additionally, ANOVA Tables S3 and S5 illustrate that temperature (linear effect) is not significant ($p > 0.05$) impact on glucose and xylose yield, while the interaction effect of reaction temperature and time was significant. Figures 5C-II & III and S7 B&C demonstrate the combined (linear and interaction) effect of reaction temperature with reaction time and solid loading on solid recovery and lignin removal yield. The response surface plots (5C-II&III) for solid recovery for reaction temperature have a slight curvature, indicating the significance ($p <.0001$) of temperature on the measured response. Similarly, the response plots (S7B&C) for lignin removal saw an increase in yield with increase in temperature, which corroborates the significant ($p <.0001$) effect of temperature. Additionally, the interaction effects from Table S3 indicates that reaction time and temperature was significant ($p = 0.0361$) on lignin removal yield and Table S4 demonstrates that reaction temperature and solid loading has significant ($p = 0.0496$) effect on solid removal yield.

Reaction time: Figures 5A-I & III and 5B-I & III demonstrate the linear and interaction effect of reaction time with reaction temperature and solid loading on glucose and xylose yield. Results from the surface plots and ANOVA (Table S3&S4) indicate that the linear effect of reaction time on glucose and xylose yield were not significant ($p > 0.05$), while interaction effect of reaction temperature and time on glucose yield was significant ($p = 0.0116$). Figures 3 5C-I & III and S7 A&C demonstrate the combined effect of reaction time with reaction temperature and solid loading on solid recovery and lignin removal yield. Results from the surface plots and ANOVA (Table S3&S4) indicate that linear effect of reaction time on solid loading on solid recovery were significant ($p < 0.0001$). However, the interaction effect of reaction time on solid loading and reaction temperature on solid recovery were not significant ($p > 0.05$).

Taken together, the results from the CCD experiments illustrate that the design specified levels for reaction time, solid loading, and reaction temperature had a significant effect on solid recovery and lignin removal yield. In addition, the interaction effect of reaction time and reaction temperature was significant on all the four measured responses.

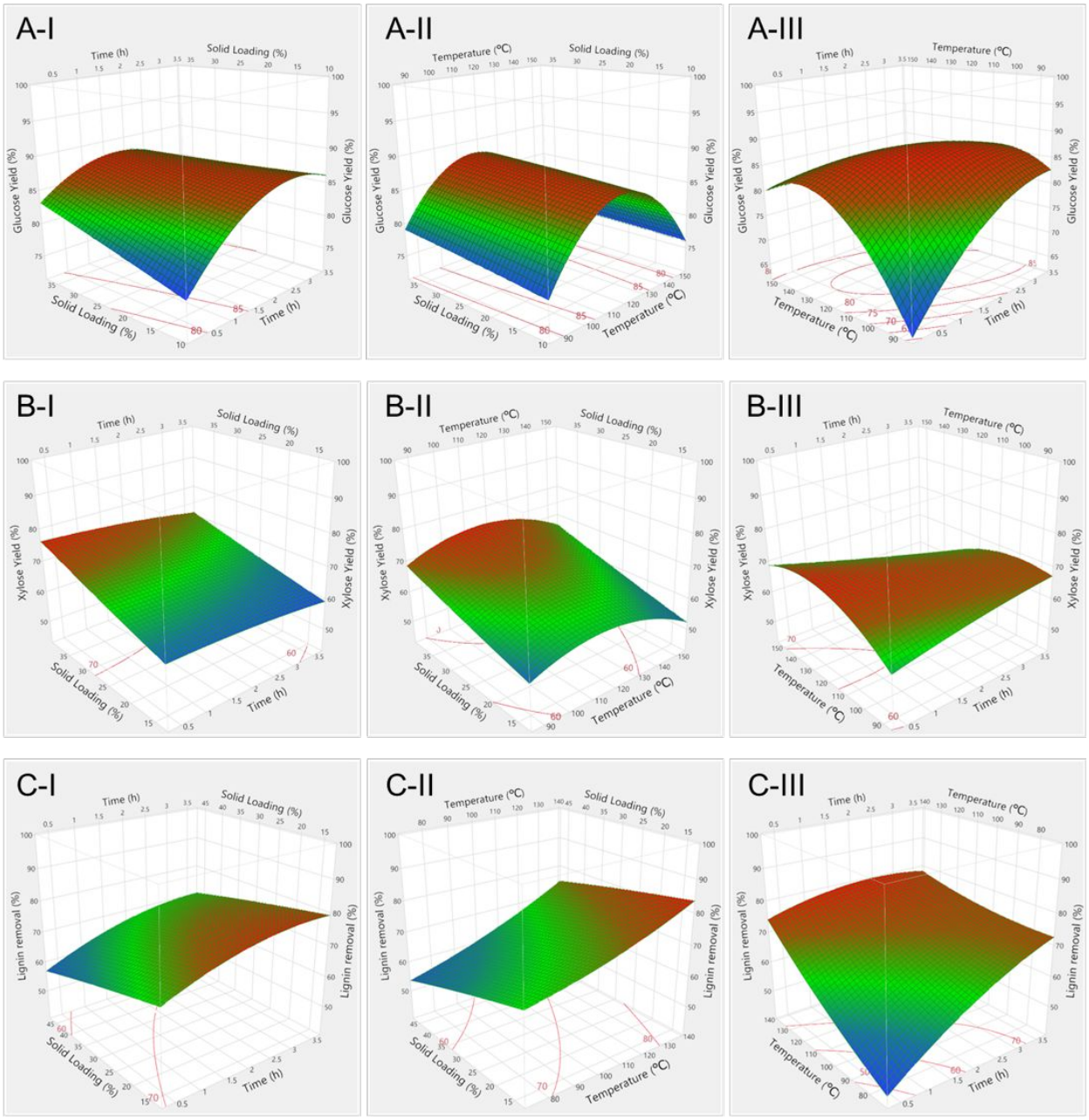

Figure 5. Surface response plots for glucose yield (A), xylose yield (B), and lignin (C) showing the effects of reaction time and solid loading (I), solid loading and temperature (II) and temperature and reaction time (III).

Process Consolidation and Scale-Up

Although four responses were surveyed, the total sugar released is the most important factor for this process since sugars are a direct metabolite utilized in the bioconversion tests to produce biofuels and bioproducts. Therefore, the glucose yield was selected as the primary point for

optimization and xylose yield was secondary. The results outlined in the previous section show that the effect of all three factors on glucose yields were not significant. Therefore, the following conditions were selected to maximize process economics (i.e., shortest time, lowest temperature, and highest solid loading), and the optimal process parameters chosen for pretreatment of sorghum biomass via ethanolamine were temperature 100 ℃, time 1h, solid loading 40%. In the future a wider range of conditions could be tested to further probe the possibility of reducing time and temperature, while increasing solid loading. Although, this additional optimization is likely going to require changes in process configuration and reactor capability. Using the model developed, this resulted in a predicted yield of 82% glucose, 72% xylose, 57% lignin removal, and 70% solid recovery, which was verified experimentally as yield of 90% glucose, 76% xylose, 59% lignin removal, and 73% solid recovery (Figure 6A). Thus, the results aligned very well with the model's prediction and further analysis of the individual independent variables on the response variables were inferred from the optimal conditions.

(A)

Optimal Parameters (T=100 °C, t=1h, SL 40%)	**% Glucose (g/L)**	**% Xylose (g/L)**
DOE Predicted Results	82.0	72.0
Verified Experimental Results	89.6	75.6
One Pot/ Parr Reactor (1L) 25% 2-aminoethan-1-ol in water	98.6 (52.7)	100.0 (28.8)

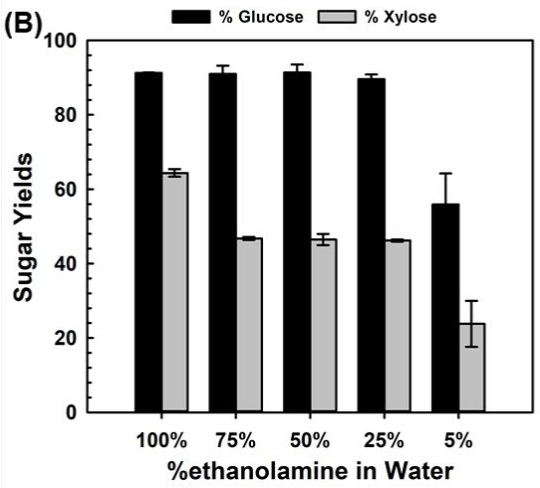

Figure 6. (A) Summary of the glucose and xylose yields for the optimal conditions at small, scale and intermediate scale and (B) Glucose and xylose yields recovered after enzymatic hydrolysis of pretreated sorghum biomass with ethanolamine and varying amounts of water.

The final point of optimization is to evaluate the impact of water within the pretreatment solvent. This directly enables the integration of downstream processes (such as enzymatic hydrolysis and microbial bioconversion) that are chemically sensitive and require water and will enable the overall biomass to biofuel process to be conducted without upfront separations, called a one-pot process

(Figure 7 and S8). These changes have obvious benefits associated with process consolidation and process intensification. Additionally, this eliminates the use of large amounts of solvents to wash the biomass after pretreatment, as well as the loss of valuable biomass components in waste streams. Figure 6B shows the impact the percentage of water present in the pretreatment solvent has on glucose and xylose yields. As the percentage of water increases from 0% to 75% (in 25% increments), glucose yields remain constant with ~90% cellulose conversion, however, there is a 45% decrease in hemicellulose conversion rate. When the water increases to 95% of the pretreatment solvent, glucose yields drop by 39%, which is also accompanied by an additional 50% reduction in xylose yields. As ethanolamine becomes more dilute (>75%), the pretreatment capability and ability to dissolve lignin/hemicellulose deteriorates. With these new results, the optimal conditions selected for pretreatment of sorghum biomass via ethanolamine were temperature 100 ℃, time 1h, solid loading 40% and 25% ethanolamine in water, implemented in a one pot configuration and scaling 40X from previous experiments.

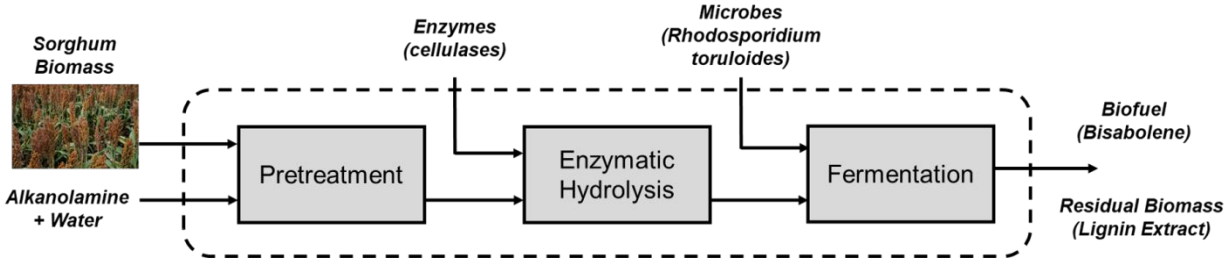

Figure 7. Process flow diagram for the one-pot conversion of sorghum biomass into biofuels using ethanolamine as a pretreatment solvent. Note: The dashed lines represent three different processes that take place sequentially in the same vessel.

The major benefit worth noting is the increase in yields obtained after process consolidation and scale up (Figure 6A). This is largely due to the new reactor utilized during scale up since the smaller scale set up did not include agitation or mixing, which mitigated mass transfer and diffusivity. The larger reactor includes a scraped wall impeller that can lift, and overturn different types of slurries and reaction media and the sugar yields are nearly 100% of the theoretical maximum, indicating a complete hydrolysis. Another important benefit is the elimination of unit operations associated with water washing and solid-liquid separation, which reduces the loss of hemicelluloses and oligosaccharides/sugars. This obvious economic and environmental benefits, but also enables process intensification. After water washing and drying pretreated biomass, the

fibers can collapse and make saccharification difficult, therefore, the solid loading for enzymatic hydrolysis is typically 2-5 wt.%. In this case, when those additional steps are eliminated, the fibers are still accessible and can be easily deconstructed by the action of the enzymes. This enables an increase in the solid loading to 15 wt.%, which corresponds to an equivalent of ~5% ethanolamine. The major obstacle limiting process intensification is the toxicity of the organic solvent, which has been potentially addressed by demonstrating the effectiveness of the solvent in the presence of 75% water. Subsequent biocompatibility tests described below in this study confirmed this hypothesis.

BIOMASS CHEMICAL AND STRUCTURAL CHARACTERIZATION

Lignin extraction efficiency and sugar release are directly correlated to pretreatment effectiveness, however, there are structural and morphological features in the biomass that can act as secondary drivers for pretreatment effectiveness.[34–36] Therefore, several analytical studies (PXRD, TGA, NMR and FTIR) were performed to evaluate the impact of pretreatment on the biomass fibers. Additionally, the residual lignin recovered after enzymatic hydrolysis was analyzed to reveal the structure and chemical functionality of the extracted lignin. The biomass depicted a lighter color after pretreatment (Figure 8A), which is typically associated with a loss in lignin, however, there are no obvious changes in morphology. Next, PXRD analysis was utilized to determine the amounts of crystalline and non-crystalline constituents and substrate features found in the sorghum samples. The PXRD spectrum reveals the changes between crystalline cellulose and amorphous cellulose, hemicellulose, and lignin, which is generally expressed as crystallinity index (CrI) (noted on each curve) (Figures 8B). Three similar peaks were observed in the diffraction patterns for the biomass samples (Figure 8B) located at about 2 thetas 16°, 22°, and 34° according to the crystallography plane of (101), (002), and (004), respectively.[37,38] These characteristic peaks are related to native cellulose (I) polymorph and the results indicate little or no change on the crystalline structure after pretreatment. Additionally, there are minimal changes in the crystallinity index (CI) (Figure 8B) after pretreatment (47.5% vs 47.2%). Further analyses using a peak deconvolution software extracted the amorphous peak and quantified the % area in relation to the crystalline peaks. This method also reveals that the amorphous contribution is relatively the same indicating no change in crystallinity (Figure S10-S11).

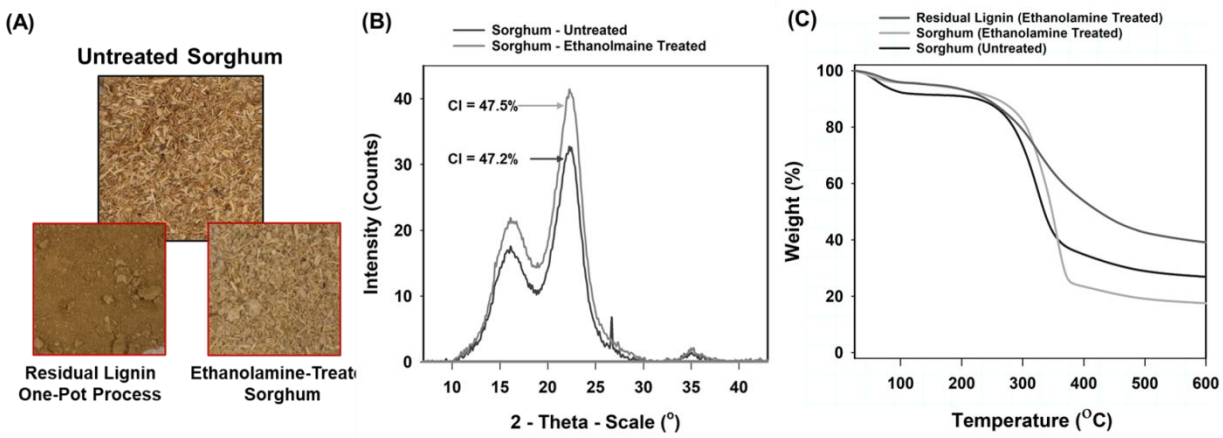

Figure 8. (A) Images of sorghum biomass changes during pretreatment and the residual lignin after the one-pot process, (B) PXRD diffractograms for the untreated and ethanolamine-treated sorghum; and (C) Thermal degradation behavior of untreated and treated sorghum fibers using TGA analyses.

Both crude and purified cellulosic preparations were further subjected to derivative thermogravimetric analysis (TGA) and differential scanning calorimetry (DSC) in a N_2 atmosphere to determine their impact of alkanolamine pretreatment on the thermal properties of the biomass. Thermal degradation tests indicate a loss of 63% by mass for the untreated biomass fibers (T=25–600 °C) (Figure 8C and S12). For the ethanolamine-treated fibers, there are two distinct regions of interest with 29% mass loss for (T=25–360°C) and 42% mass loss for (T= 360–600°C). Together, this indicates a loss of 71% by mass for the biomass fibers after heat treatment (Figure S12). Therefore, the results depict a reduction in thermal stability for the biomass fibers after pretreatment. The primary region of interest is (T=150–500 °C), which is associated with removal of linked water and lignin, hemicellulose, and cellulose. The lower temperature range (T=150–350 °C) is related to the thermal degradation of hemicellulose and some portions of lignin, while T=310–400 °C is related to the thermal degradation for cellulose and lignin, and almost complete cellulose decomposition. Note: (T<100 °C) is usually due to residual water or volatile organics and is negligible while lignin (due to its phenyl groups), has a wider temperature degradation range of T = 200–700 °C, when compared with hemicellulose and cellulose (see figure S15 for a comparison to commercial biopolymers). Based on the pretreatment results, a large amount of lignin was extracted after pretreatment (~80%). Since lignin is a significant contributor to high thermal stability, loss of lignin will result in a reduction in thermal stability of the biomass fibers.

In addition, the lignin extract recovered after pretreatment was analyzed and indicated a loss of 54% by mass of the biomass fibers after heat treatment (Figures 8C and S14). This is expected due to the higher thermal stability expected for lignin and is similar to that observed in the commercially available lignin extract (organosolv lignin) (Figure S14).

FTIR spectra of the biomass samples in the wavelength region from 4000 to 600 cm^{-1} were also collected to study changes in the chemical functional groups present in the pretreated biomass and the residual lignin. Figure 9 shows the FTIR of the raw biomass, the pretreated biomass, and the lignin recovered after enzymatic hydrolysis (key peaks are summarized in Table S9). The IR spectra of untreated sorghum show strong bands associated with hydrogen-bonded O–H stretching absorption around 3300 cm^{-1} and a notable C–H stretching absorption around 2900 cm^{-1}.[39] In the fingerprint region, between 1,800 and 600 cm^{-1}, several absorption bands that are connected with various vibrational modes in carbohydrates and lignin are also present in sorghum (see Table S9). In particular, there is a distinct band at ~1710-1,734 cm^{-1} for the raw biomass sample, which has been related to saturated alkyl esters from hemicellulose, as well as, some phenolics.[40–42] This peak in the FTIR spectrum is no longer pronounced after pretreatment, which supports our results indicating removal of lignin and hemicellulose by the pretreatment. There are also important phenolic peaks observed as a doublet at ~1,600 to 1,634 cm^{-1} in all samples. The band at ~1,638 cm^{-1} has been assigned to an aromatic stretch, and the band at ~1,604 cm^{-1} with the α–β double bond of the propanoid side group in lignins.[40,41] These bands are present in the untreated biomass, but greatly diminished in the pretreated biomass (although not completely removed), which is in line with our observations for lignin removal. Although the pretreatment resulted in high lignin removal (~75-80 %), the ethanolamine solvent did not completely remove lignin, hence the observed peaks.

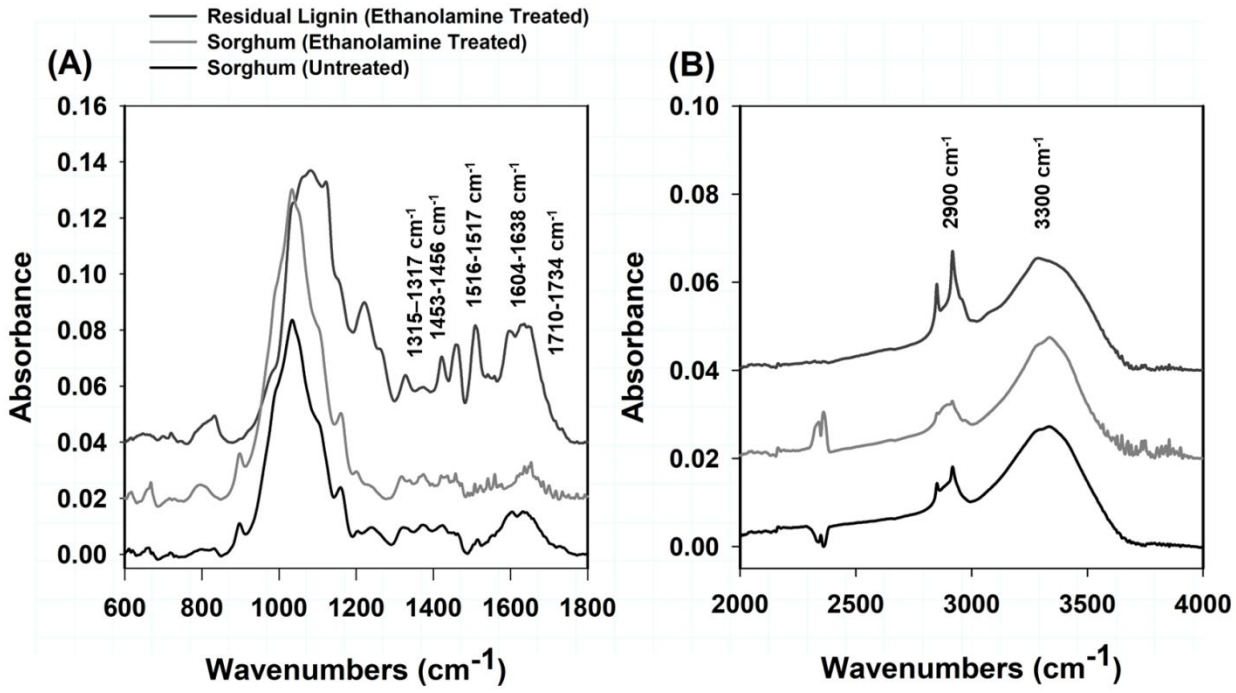

Figure 9. FTIR spectra of sorghum before and after ethanolamine-based pretreatment (A) in the fingerprint region (600–1,800 cm^{-1}) and (B) the region (2000–4000 cm^{-1}).

For the lignin sample recovered, the phenolic peaks observed at ~1,600 to 1,634 cm^{-1} are highly emphasized and increase in absorbance compared to the raw biomass (Figure 9A). An important characteristic of the lignin extract is the type of lignin. Sorghum is a grassy species, and has two main types of lignin (guaiacyl and syringyl rings).[43] These rings are observed as aromatic skeletal vibrations of the benzene ring at ~1,513–1517 cm^{-1} bands, with specific heightened absorbance for guaiacyl ring-related bands observed at 1,516–1,517 cm^{-1} (Figure 9A).[39,40,42,43] This suggests that the syringyl/guaiacyl (S/G) ratio is low and less than 1. While FTIR is a simple non-destructive technique that can be utilized to obtain quick and accurate information about the structure of lignin, it is largely qualitative. Therefore, additional experiments were carried out utilizing ^{1}H–^{13}C HSQC NMR to obtain a semiquantitative lignin analysis and to accurately quantify S/G ratios.

Using heteronuclear NMR analysis, key lignin monolignol subunits were revealed and assigned using previously published spectra (Figure 10, S18, Table S10).[44–46] The aromatic region (~6.0–8.0/100–150 ppm) of the lignin samples, depict the placement and composition of S, G (including H-type lignin (p-hydroxyphenyl)), and tricin units (T) incorporated in the extracted lignin (Figure

10). The NMR spectra show that the lignin extract is largely dominated with G-units (74%) followed by S-units (23%) and trace amounts of tricin (<1%) (Figure 10, S18, Table S10). Eudes *et. al.* report that the lignin composition of wild type sorghum is 67% G, 28% S and 5% T with a S/G ratio of ~0.41.[45] Following the ethanolamine pretreatment, the resultant S/G ratio is ~0.32 of the lignin extract. Although this S/G ratio is similar to the wild type of lignin, the results depict an increase in G-units as well as loss of tricin after pretreatment. It is important to also note that the lignin extract is free from condensed lignin, which is typically observed after pretreatment with some organic solvents, ionic liquid, deep eutectic solvents.[44,47,48] While condensed lignins are usually characterized with increased thermal stability,[44] they are very difficult to degrade and are undesired for applications where easy lignin depolymerization is desired. Therefore, the lignin extract recovered after ethanolamine pretreatment is likely amenable for downstream lignin depolymerization and valorization (chemically and/or biologically). Lastly, the aliphatic region (2.5–6.0/50–90 ppm) of the lignins, revealed the lignin inter-units and side chains (Figure S18). The recovered lignin extract is largely dominated by β-O-4′ units with race amounts of β-5′ and β-β′ units (Figure S18). These linkages are expected and have been reported in lignin from other grassy species (like switchgrass and corn stover).[28,46]

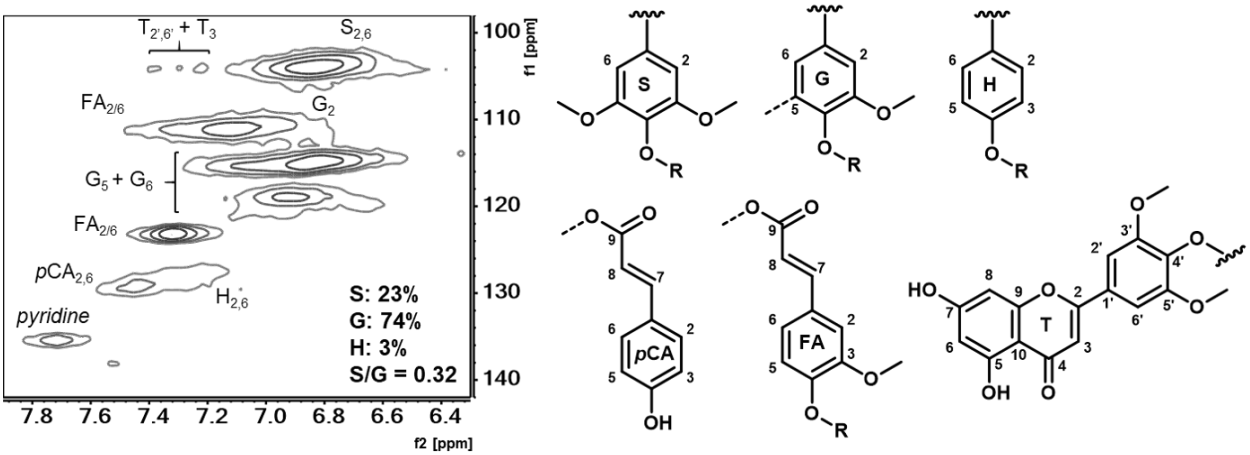

Figure 10. Lignin monomeric composition in lignin extract analyzed by 2D ^{13}C–^{1}H HSQC NMR spectroscopy showing the aromatic region (~6.0–8.0/100–150 ppm). Lignin monomer ratios including tricin (T) are provided on the figures. S: syringyl, G: guaiacyl, H: p-hydroxyphenyl, *p*CA: *p*-coumarate, FA: ferulate.

BIOCONVERSION OF HYDROLYSATE

In order to demonstrate the utility of this hydrolysate for downstream bioconversion into valuable bioproducts, we utilized the oleaginous yeast *Rhodosporidium toruloides* which we have previously engineered to produce the biofuel bisabolene (Figure 11A).[49] This basidiomycete fungi can be cultivated at high cell densities while efficiently co-utilizing a broad array of carbon sources commonly found in cellulosic hydrolysates.[49] It is particularly notable for its resistance to high concentrations of ILs/organic solvents that are normally toxic to other organisms.[50] For the bioconversion tests, two replicas (hydrolysates 1 and 2) of the ethanolamine-derived hydrolysates were utilized as the sole carbon sources for bioconversion into bisabolene over a course of 94 hours. *R. toruloides* was also cultivated in the standard rich yeast growth media YPD as a control. The cells were capable of robust growth in both hydrolysates, achieving final OD_{600nm} of 8.4 ± 1.2 and 7.6 ± 0.8 in hydrolysates 1 and 2, respectively. This was significantly higher than the ending OD_{600nm} achieved in YPD of 3.4 ± 0.2 (p = 2E-3 and 7E-4 for hydrolysates 1 and 2 respectively). Growth rates over time suggest a longer lag time and slower growth rate of cells in both hydrolysates relative to cells in YPD (Figure S19), suggesting the organism needed to adapt to the hydrolysate conditions, a common observation of organisms grown in rich media seed cultures.

R. toruloides could produce appreciable levels of bisabolene, achieving titers of 1129 ± 27 and 1181 ± 49 mg/L in hydrolysates 1 and 2 respectively (Figure 11B). These titers were significantly higher than the 125 ± 16 mg/mL titer achieved in YPD (p = 7E-6 and 4E-6 for hydrolysates 1 and 2 respectively). Notably, these titers are also substantially higher than those achieved originally by Yaegashi *et. al.*, which utilized this strain to produce ~261 mg/L of bisabolene at bench scale from a corn stover hydrolysate produced using choline a-ketoglutarate IL.[49] Rodriguez *et. al.* also achieved 135mg/L of bisabolene from the IL pretreatment of milled *Arabidopsis.*[51] For the ethanolamine-derived hydrolysates, *R. toruloides* consumed virtually all glucose in both replicates, and virtually all of xylose in hydrolysate 1, and 74% of the xylose in hydrolysate 2 yielding an average consumption of 98.5% glucose and 87.4% xylose (Figure 11C). In addition to sugar consumption, *R. toruloides* was also able to consume different metabolites found in the hydrolysate. The results of Yaegashi *et. al.* demonstrate *R. toruloides* consumption of lignin-related aromatic compounds such as (*p*-coumaric acid, *p*-hydroxybenzoic acid (4-HBA), ferulic acid, vanillic acid, or benzoic acid) with emphasis on *p*-coumaric acid as the naturally occurring

phenolic from the biomass.[49] In the case of the ethanolamine-derived hydrolysate, large amounts of benzoic acid (~810 mg/L) along with small amounts of other aromatic compounds (4-HBA, vanillic acid, ferulic acid and vanillin) were detected after pretreatment and were completely consumed by *R. toruloides* (Figures 11D and S20). In addition, the ethanolamine-derived hydrolysate contained large amounts of acetic acid (3.5 g/L), lactic acid (1.5 g/L) and furfural (2.5 g/L) (Figures 11D, S21-22). Following *R. toruloides* bioconversion, the organic acids were also fully consumed, along with, ~49% consumption of furfural, while the ethanolamine levels remain relatively unchanged (Figure S22).

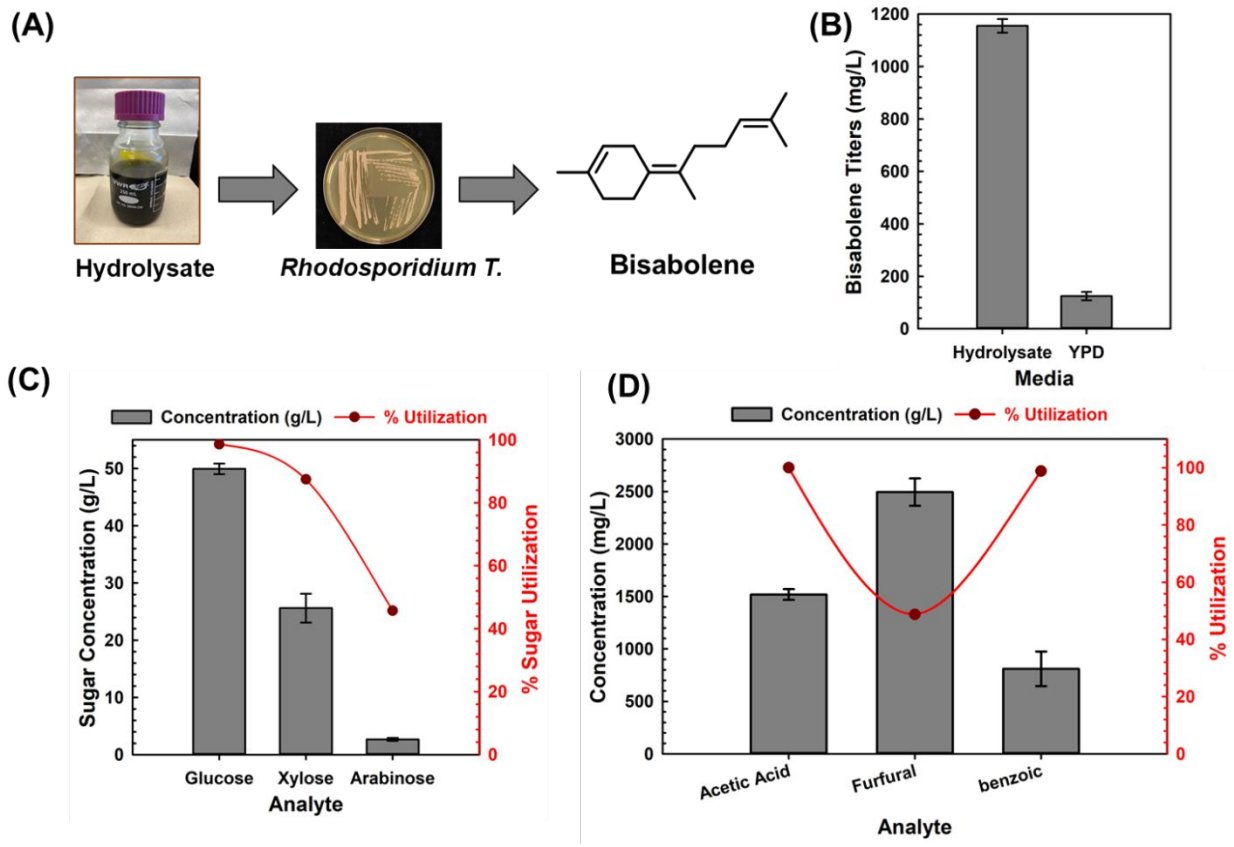

Figure 11. Bioconversion by *Rhodosporidium toruloides* of hydrolysates. A) The replica hydrolysates (1 and 2) were used to cultivate *R. toruloides*, a yeast engineered to produce the biofuel bisabolene from lignocellulosic feedstocks. (B) Average titers of bisabolene recovered after bioconversion, compared to standard *R. toruloides* YPD growth media. (C) Average sugar, (D) phenolic/acid/furan composition and utilization of each hydrolysate.

BIOFUEL SELLING PRICE AND ECONOMIC IMPACT OF BIOMASS DECONSTRUCTION

We conducted a technoeconomic analysis to explore the impact of the alkanolamine-based pretreatment on biorefinery economics and to identify key cost drivers. The first goal was to compare the ethanolamine-based deconstruction process with other promising biomass deconstruction processes such as those based on cholinium lysinate [Ch][Lys] and ethanolamine acetate [EOA][OAc].[14] Compared to ethanolamine acetate, the results for ethanolamine-based deconstruction presented reduced the biomass deconstruction cost, excluding biomass feedstock cost, by 50% (Figure 12). This large reduction is primarily due to the 33% higher sugar yield found in this study, which was also recovered with lower temperature, higher solids loading, lower solvent loading and half the enzyme loading compared to the ethanolamine acetate-based biomass deconstruction process. Compared to cholinium lysinate, this study demonstrated higher sugar yields and ethanolamine has a 28% lower unit cost ($1.45/kg vs $2/kg); this translates to a 24% lower biomass deconstruction cost. The higher biomass-to-sugar conversion rate demonstrated for ethanolamine is primarily owed to the ease of lignin removal that was achieved at these conditions (see section on solvent screening). In each case, the process chemicals and enzymes required for biomass pretreatment and a subsequent saccharification contribute to more than 95% of the total biomass deconstruction cost (Figure 12). This highlights the importance of reducing the cost of process chemicals used during biomass deconstruction.

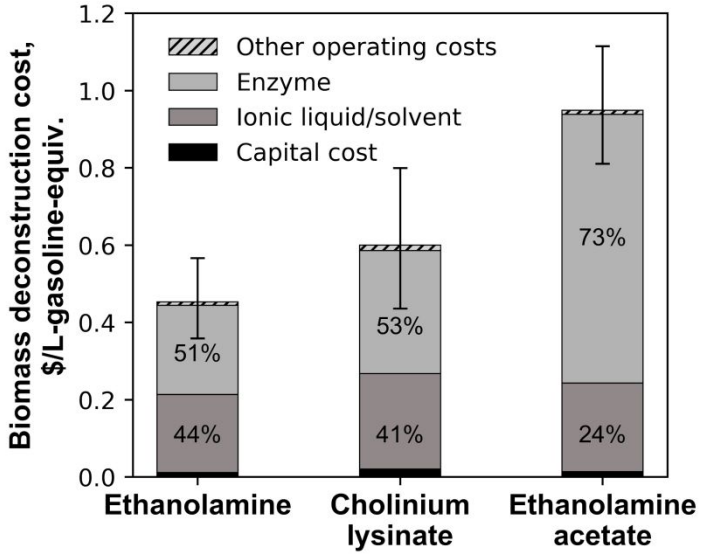

Figure 12. Biomass sorghum deconstruction cost with ethanolamine, cholinium lysinate, and ethanolamine acetate. For this comparison, we used the same biomass feedstock composition (ESI-Table 11) but excluded the biomass feedstock cost. Experimental data for cholinium lysinate[52] and ethanolamine acetate [14] were gathered from prior studies. Ionic liquid loading rates of 10 and 15 wt% (based on the whole slurry) and the enzyme loading rates of 10 and 20 mg/g of dry biomass were considered for cholinium lysinate[52] and ethanolamine acetate[14], respectively. Other operating costs include utilities, maintenance, and property taxes. Error bars represent the impacts on the biomass deconstruction cost when the solvent recovery rate varies from 90 to 99% without changing other input parameters.

To contextualize the deconstruction results within a full biorefinery, results were generated for two biofuels: ethanol and bisabolane (a potential jet fuel blend stock produced by hydrotreating microbially-produced bisabolene).[53] The performance of the ethanolamine-based biomass deconstruction process demonstrated in this study results in a minimum ethanol selling price at the biorefinery gate of $1.7/L-gasoline-equivalent ($6.3/gge). For comparison, a prior study reported a minimum selling price of ethanol equal to $1.45/L-gasoline-equivalent when biomass is pretreated using an typical organosolv process, although this value is not directly comparable to ours because that study used a biomass feedstock cost considerably lower than what is included in our modeling results.[54] The biomass feedstock cost (35%), biomass deconstruction (27%), ethanolamine recovery (13%) are the major contributors to the ethanol production cost (Figure 13A). The current minimum selling price of ethanol at the biorefinery gate is 2.8 times greater than the last 10-year (2010-2019) average-selling price of gasoline at the refinery gate of $0.59/L ($2.2/gal). However, the minimum ethanol selling price could reach to $0.6/L-gasoline-equivalent ($2.4/gge) in an optimal future case (Figure 13A). This future optimal case is based on a high quality biomass sorghum with the total carbohydrate content of 70 wt% (30% more than the state-of-the-art (SOT) scenario) and a high ethanol yield of 95% of the theoretical yield (5% more than the SOT scenario).[55] Both of these parameters increase the production volume of ethanol and are most influential to the ethanol production cost. While this study demonstrates a biomass-to-sugar conversion rate of more than 99% of the theoretical potential, there are further process improvement opportunities, specifically achieving the same sugar yield with a lower ethanolamine loading of 10 wt% (based on the whole slurry), with a lower enzyme loading of 7 mg-protein/g-biomass, and a shorter hydrolysis time of 48 h. The future case scenario considers these targeted

operating conditions to reduce the cost contribution from the biomass deconstruction stage. In addition, an improved biomass sorghum production and supply system—higher biomass yield of 28 bdt/ha, sustainable farming with a low fertilizer application, and best management practices to reduce handling and truck waiting hours—demonstrated in our recent study are considered to reduce biomass feedstock cost from $124/bdt to $70/bdt.[56] Step-by-step reductions in the delivered biomass feedstock cost are presented in our recent study. These system wide improvements are essential to reduce the overall ethanol production cost and requires further research and development efforts.

In contrast to ethanol, bisabolene production from the lignocellulosic hydrolysates is at a very early stage of development. This study demonstrates whether it is worth optimizing the bisabolane (hydrogenated product of bisabolene and jet fuel equivalent molecule) production process. Our experimental results show the bisabolene yield from simple sugars of 5.9% of the maximum theoretical yield.[57] This low yield unsurprisingly results in a high bisabolane selling price at the biorefinery gate of $34.5/L-Jet A-equivalent (Figure 13B). Increasing the bisabolene yield to 50% and 90% of the stoichiometric theoretical yield—assumed based on the demonstrated yield of other biofuels such as ethanol[58]—dramatically reduces the minimum selling price of bisabolane to $4.2/L-Jet A and $2.4/L-Jet A, respectively. This highlights the importance of the yield improvement to reduce the minimum selling price of biofuel. More importantly, the intermediate yield improvement could substantially reduce the selling price of bisabolene. In addition to the improved yield of 90% of the theoretical yield, exploring the optimal conditions described above (e.g., high-quality sorghum, low-cost feedstock, lower residence time) can reduce the bisabolene-selling price to $0.9/L-Jet A-equivalent (Figure 13B). Achieving a price competitive with jet fuel's 10-year average price of $0.6/L requires policy support or lignin valorization to the high-value chemicals.[53] The analysis also shows that ethanolamine recovery is essential to reduce the biofuel production cost. Reducing ethanolamine recovery from 95% to 80% (equivalent to 5 times uses and then disposal) increases the state-of-the-art ethanol and bisabolene selling prices by 21% and 16%, respectively (Figure 13). In addition, the impact of ethanolamine recovery can be minimized by reducing its loading rate. For instance, at a lower ethanolamine loading of 10 wt% (instead of 15%), increasing ethanolamine recovery from 95% to 99% decreases ethanol and bisabolane production costs by 2%. Note: Concurrent studies utilizing variants of this strain have been able to produce higher titers from lignocellulosic hydrolysates, so we expect with further process

optimization in bioreactors, the bisabolene titers can also be improved using hydrolysates derived from this process.[50] In addition, the strain used in this study is in an early stage of development and further strain engineering will enable improvement of titers towards the targets outlined by the technoeconomic analyses below.[59]

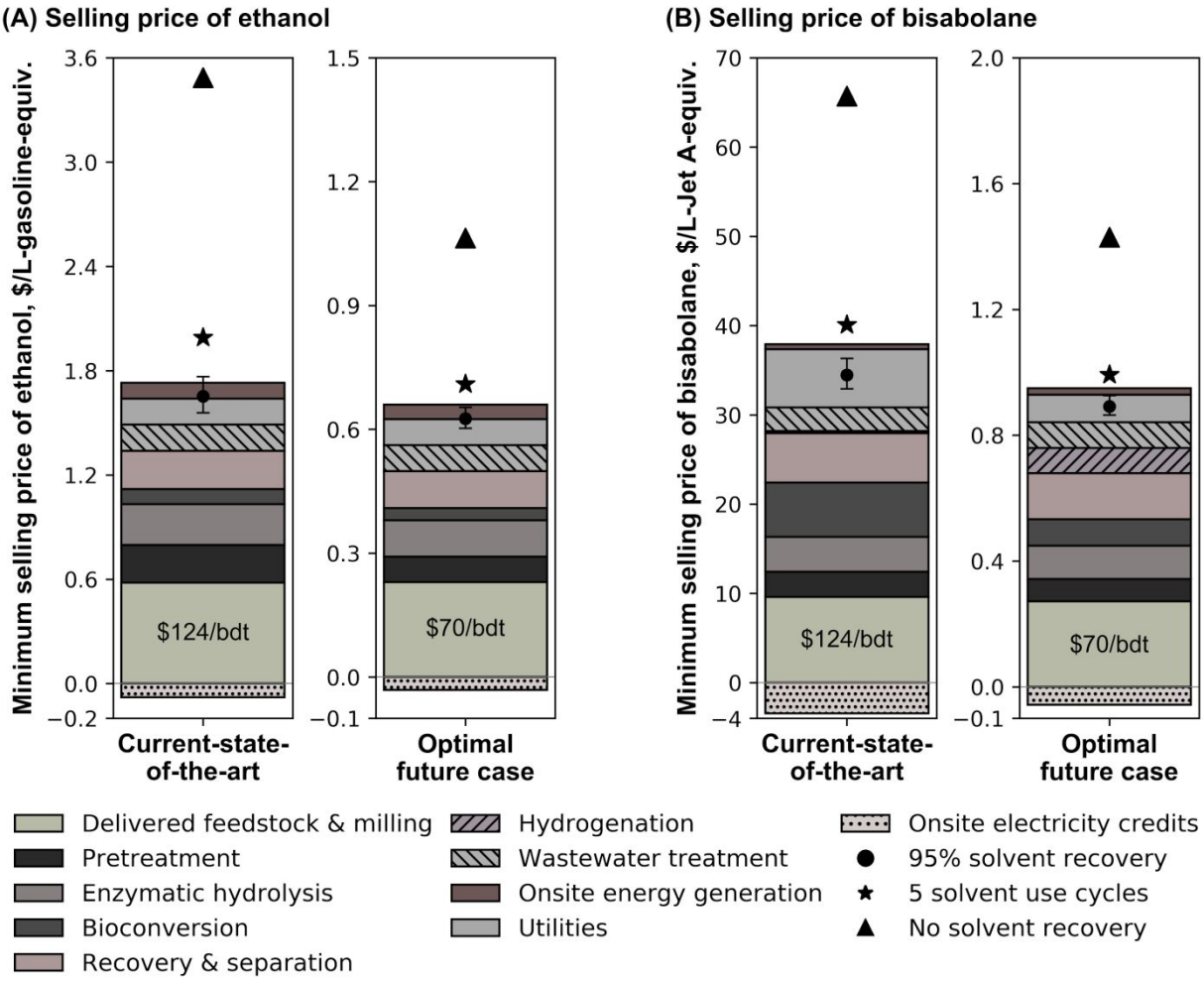

Figure 13. Minimum selling prices of ethanol (A) and bisabolane (B) at current state-of-the-art and optimal future case scenarios. Bisabolane is the jet fuel equivalent hydrogenated product of bisabolene. The hydrogenation cost is relatively small ($0.22/L-Jet A) due to a low bisabolene yield at the current state-of-the-technology. The annual operating cost is documented in the ESI-Table S12. In this figure, the process electricity costs are included in each stage and, separately, the total generated electricity on-site is considered as a credit (using the same per-kWh electricity

cost). The presence of an electricity credit bar does not necessarily suggest that the facility is a net exporter to the grid.

CONCLUSIONS

This work demonstrates the feasibility of applying dual functional solvents called alkanolamines towards the conversion of biomass to biofuels. Several key factors were considered to effectively integrate the pretreatment technology into a biorefinery, including solvent screening, effectiveness on a broad range of feedstocks, fractionation of lignocellulose components, solvent cost, generation of biomass-derived enzyme and microbe inhibitors, and bioconversion efficacy. To initiate the investigation, several molecular solvents with similar functionalities were studied for their pretreatment effectiveness, in terms of lignin/hemicellulose removal and enzymatic hydrolysis yield. Several different alkanolamines were screened using COSMO-RS models to understand their potential for lignin/hemicellulose removal, as well as their mechanisms of action that promote effective pretreatment. The results show that both amine and hydroxyl functionality play an important role in controlling lignin removal, however, the amine group was more important. Simple changes in amine functionality (based on number of amines, degree of substitution, and confirmation) proved to significantly influence pretreatment effectiveness. The lower pretreatment capability of the tertiary amine (N, N-dimethylethanolamine) is due to the reduced polarity, which leads to a weaker interaction between lignin and tertiary amines. In addition, amine dominated solvents (1,3-diamino-2-propanol) had stronger affinity to interact with hydrogen bond donor groups of lignin than the hydroxyl dominated solvent (2-amino-1,3-propanediol). COSMO-RS was also used to develop a predictive model for lignin removal based on the several influential quantities: H^E, $\ln(\Upsilon)$), viscosity and pK_a. A comparison of the predictive model and experimental results shows that they are in excellent agreement. Three amines emerged from this screen as the most effective for pretreatment (ethanolamine, 1-amino-2-propanol and 2-(methylamino)ethanol) and ethanolamine was selected for future screening and process development.

Ethanolamine was further evaluated for its effectiveness at pretreating various biomass types, which revealed that sorghum (grassy) along with hardwoods (almond, walnut) are easier to deconstruct than softwood (pine, fir). Sorghum was selected for further process optimization due to its high glucan content. Using DOE methodology, three factors (pretreatment time, temperature,

and solid loading) were screened across four levels (glucose, xylose, lignin removal, and solid recovery). The results were not significant within the range tested for glucose yields, but low severity process parameters were identified, and it was found that the pretreatment process can tolerate high water content (up to 75%), both of which enable process consolidation and intensification to reduce costs. The pretreated biomass and recovered lignin were studied using PXRD/TGA/FTIR/NMR analysis and the characterization revealed that the morphology and crystallinity of biomass does not change after pretreatment, and recovered lignin is dominated by guaiacyl groups. This lignin is less condensed compared to other pretreated lignins, so should be amenable to catalytic upgrading into valuable products. With the final selected conditions, the pretreatment was scaled up, resulting in nearly 100% deconstruction efficiency for enzymatic hydrolysis. Bioconversion tests to produce the jet fuel precursor bisabolene were performed on these hydrolysates at the benchtop scale using engineered *R. toruloides* in which over a 1 g/L bisabolene titer was achieved. Overall, this study has demonstrated the effectiveness and robustness of alkanolamines for use in economic biomass pretreatment and presents a new solvent group to be considered for use within commercial biorefineries.

MATERIAL/METHODS

MATERIALS

The main biomass utilized was Sorghum (*Sorghum bicolor)* which was donated by Idaho National Labs (Idaho Falls, Idaho, USA). The biomass was dried for 24 h in a 40 ºC oven. Subsequently, it was a knife-milled with a 2 mm screen (Thomas-Wiley Model 4, Swedesboro, NJ). The resulting biomass was then placed in a leak-proof bag and stored in a cool dry place. Additional biomass studied include the forest residues generated from California woody biomass such as pine, walnut, almond, fir. These feedstocks were generously donated by Aemetis, Inc. (Cupertino, CA). They were also prepared and stored using similar conditions (dried for 24 h in a 40 ºC oven). The following alkanolamines were purchased from Sigma Aldrich (St. Louis, MO) and used as received: ethanolamine (≥99% purity), 1-amino-2-propanol (93% purity), 2-(Methylamino)ethanol (≥98% purity), N,N-dimethylethanolamine, (≥99.5% purity), 1,3-diamino-2-propanol (96.5%), 2-amino-1,3-propanediol (98% purity), citric acid (ACS reagent ≥99.5%), sodium citrate tribasic dihydrate (ACS reagent, ≥99.0%) and sodium azide. Sulfuric acid (72% and

95-98%) was purchased from VWR), and sugar standards glucose (≥99.5%), xylose (≥99%), and arabinose (≥98%) were procured from Sigma-Aldrich for high-performance liquid chromatography (HPLC) analysis. Commercial cellulase (Cellic® CTec3) and hemicellulase (Cellic® HTec3) mixtures were provided by Novozymes, North America (Franklinton, NC).

METHODS

Biomass Pretreatment

The biomass pretreatment was carried out using the conventional method that involves early separation (or washing) to remove the solvent after pretreatment (prior to downstream conversion). In a typical experiment, 1 g of the biomass and the solvent was loaded into an ace pressure tube (50 mL, Ace Glass Inc., Vineland, NJ) and homogenized. The solid loading was controlled at 20 wt% and heated in an oil bath set to 140 ºC for 3 h. After pretreatment, the mixture was allowed to cool for 30 mins and then washed 5 X with deionized water using a 40 mL centrifugation-decanting cycle. Finally, the recovered solid fraction was lyophilized and then gravimetrically tracked to determine the solid recovery (SR), while also passing through enzymatic hydrolysis (EH) and compositional analysis (CA). All the experiments were performed in duplicate, and the average values are detailed here. The solid recovery (%SR) after pretreatment was calculated based on the following equation. The selection of the initial conditions was based on previous results demonstrating pretreatment effectiveness and loosely based on the pretreatment severity factor. [14,33,60] Additionally optimization on various factors such as pretreatment time, temperature and the solid loading was conducted (see below).

$$\%\ Solid\ Recovery\ (\%SR) = \frac{Weight\ of\ biomass\ recovered\ after\ pretreatment}{Weight\ of\ biomass\ used\ for\ pretreatment} \times 100 \qquad (1)$$

Enzymatic Hydrolysis

The enzymatic saccharification of pretreated and untreated biomass was carried out using commercially available enzymes, Cellic® Ctec3 and Htec3 (9:1 v/v) from Novozymes, at 50 °C in a rotary incubator (Enviro-Genie, Scientific Industries, Inc.). All reactions were performed at 1.5 wt% biomass loading in a 15 mL centrifuge tube (using 0.15 g of the pretreated or untreated biomass). The pH of the mixture was adjusted to 5 with 100 mM sodium citrate buffer supplemented with 0.1 wt% sodium azide to prevent microbial contamination. The total reaction

volume included a total protein content of 20 mg/g biomass. The amount of sugars released was analyzed on an Agilent HPLC 1260 infinity system (Santa Clara, California, United States) equipped with a Bio-Rad Aminex HPX-87H column (300 × 7.8 mm^2) and a Refractive Index detector. An aqueous solution of sulfuric acid (4 mM) was used as the eluent (0.6 mL/min, column temperature 60 °C). All enzymatic saccharification was conducted in duplicate. The sugar yield was calculated as an overall process yield using the formula below (equation 2), which accounts for sugars/oligosaccharides lost during pretreatment/washing.

$$\%\, Sugar\ Yield\ (Process) = \%SR\ \times \frac{Weight\ sugars\ released\ after\ hydrolysis}{Weight\ of\ sugars\ in\ the\ original\ biomass} \qquad (2)$$

Compositional Analysis

The biomass compositional analysis of pretreated and untreated biomass sorghum was performed to determine the glucan, xylan, lignin, ash and extractive content by utilizing the two-step acid hydrolysis procedure previously described by NREL.[61] Dried biomass samples were extracted sequentially using the solvents: water, 80% ethanol/water, and acetone.[62] Typically, 1 g of biomass was combined to a tube containing 40 mL of the solvent of choice. The mixture was then homogenized, sonicated for 20 minutes, and then centrifuged (10 min, 4000 RPM) to separate the extracts/solvents from the residual biomass. This extraction cycle was carried out 5 times for each biomass/solvent. Finally, the residual biomass was dried overnight at 40 °C and utilized for further compositional analyses. In summary, 150 mg of the dry extractive-free biomass was exposed to 1.5 mL of 72% w/w H_2SO_4 and incubated at 30 ºC for 1 hr. Subsequently, the mixture was taken through secondary hydrolysis at 4% w/w H_2SO_4 at 121 ºC for 1 hr. After the two-step acid hydrolysis, the hydrolysates were filtered using medium porosity filtering crucibles. The filtrates were then spectrophotometrically analyzed for the acid-insoluble lignin (ASL) (NanoDrop 2000, Thermo Fisher Scientific, Waltham, MA) using the absorbance at 240 nm. Additionally, monomeric sugars (glucose and xylose) were determined by HPLC using an Agilent 1200 series instrument equipped with a refractive index detector and Bio-Rad Aminex HPX-87H column, coupled with a guard column assembly. Product separation was obtained at 60 °C with 4 mM H_2SO_4 as a mobile phase at a flow rate of 0.6 mL/min. Finally, the Klason lignin (acid-insoluble lignin - ASL) was determined gravimetrically by subtracting the weight of the oven-dried residual solids (105 ºC) and the ash content (575 ºC). All compositional analyses were conducted in

duplicate. The amount of lignin removed can be calculated using the formula below (equation 3). Note: % Lignin = %AIL + %ASL.

$$\%\ Lignin\ Removal = 100 - \%SR\ \times \frac{\%Lignin_{after\ biomass\ pretreatment}}{\%Lignin_{original\ biomass}} \quad (3)$$

Design of Experiment and Statistical Analyses

The central composite design (CCD) is a commonly used response surface methodology, and is usually used to evaluate the impact of independent variables on the measured response.[63] Unlike factorial designs, CCD requires fewer experimental runs with the capability to understand the overall (linear, interaction, and quadratic) effects of independent variables. Typically, CCD design consists of 2^p factorial runs with 2p axial runs and P_c center runs to optimize process parameters. In this study three independent variables, time (X_1), temperature (X_2) and solid loading (X_3) were selected with 8 factorial points, 6 axial points and 2 replicates at the center points resulting in 16 experimental conditions. All the experiments were performed in triplicates. Low and high levels of the independent variable was coded as -1 and +1 and axial points are located at (±α, 0, 0), (0, ±α, 0) and (0, 0, ±α) where α is the distance of the axial point and makes the design rotatable. In this study, α value was fixed at 1.682 (rotatable). The center points are used to determine the experimental error and the reproducibility of the data. The experimental sequence was randomized to minimize the effects of uncontrolled errors. The effect of three independent variables were used to develop a second-degree polynomial model (equation 4) for the response variables of glucose (Y_1), xylose (Y_2), lignin yield (Y_3), and solid recovered (Y_4). The design matrix generation and model fitting were performed in JMP Pro 14 (SAS Institute, Inc., Cary, N.C.).

$$\hat{Y} = \beta_0 + \sum_{i}^{n} \beta_i x_i + \sum_{ii}^{n} \beta_{ii} x_i^2 + \sum_{i=1}^{n-1} \sum_{j=i+1}^{n} \beta_{ij} x_i x_j \quad (4)$$

Where $\hat{Y}$ is the predicted response, β_0 the constant coefficient, β_i the linear coefficients, β_{ij} the interaction coefficients, β_{ii} the quadratic coefficients and x_i, x_j are the coded independent variables.

Table 1: Experimental factors and their coded levels of independent variables in the CCD design

Factors	Code	Coded variable levels				
		-α	**-1**	**0**	**1**	**+α**
Time (h)	X_1	**0.32**	**1**	**2**	**3**	**3.68**
Temperature (°C)	X_2	**86.36**	**100**	**120**	**140**	**153.64**
Solid loading (%)	X_3	**13.18**	**20**	**30**	**40**	**46.82**

Process Consolidation and Scale up

The integration and consolidation of the major unit operations required for converting biomass into biofuels into a single vessel is a significant process improvement strategy that is necessary to improve process economics and efficiencies. However, downstream processes are typically intolerant to high loading of organic solvents. Therefore, the addition of water into the system as a co-solvent with the alkanolamine was studied. Pretreatment experiments were carried out while varying the amount of organic solvent used in the presence of water [100, 75, 50, 25, 5] wt. %. Once an optimal range was identified the process was finally scaled up to test the performance of the process (one-pot pretreatment and saccharification) in an industrial scale pressurized reactor. Biomass pretreatment parameters were adapted from the optimized conditions identified. In a typical experiment, the biomass and pretreatment solvent were loaded into a 1 L 4520 Parr bench top reactor (Parr Instrument Company, Moline, IL, USA) equipped with three-arm, self-centering anchor with PTFE wiper blades.

Initial biomass loading was 40 g in the 1 L vessel and the pretreatment vessels were loaded with 40 wt% biomass and 60 wt% liquid, with the liquid fraction consisting of 75% DI water and 25% ethanolamine. During pretreatment, the reaction vessels were heated to a reaction temperature of 100 °C for 1 h under completely mixed conditions. Subsequently, the reactors were cooled and adjusted to pH 5 with 5 M H_2SO_4. Next additional DI water was added to reach 15 wt% solids as measured by the initial solids loading. An enzyme mixture of Cellic® CTec3 and HTec3 at ratio

of 9:1 v/v, respectively, was used at a total enzyme loading of 10 mg/g biomass dosing. The reaction vessels were completely mixed and heated to 50 °C for 72 hours. Once complete, the mixture was filtered using a 0.22 um screen and the liquid fraction was reserved for bioconversion studies and characterized for sugars, acids, phenolics and furans. On the other hand, the solid fraction was recovered for lignin analysis (see below). The recovered lignin extract i.e., the residual solid after pretreatment and enzymatic hydrolysis (in a one pot setting) was then cleansed and purified to minimize the presence of residual sugars, phenolics or organic solvent. The recovered solid fraction was water washed and returned to a neutral pH, subsequently the lignin was enzymatically treated to ensure complete removal of any polysaccharides. Finally, the recovered solid was cleansed again, centrifuged, and lyophilized to recover a sugar-free lignin powder (see Figure X).

Chromatographic Techniques

Monomeric sugars, organic acids, and furans: All monomeric sugars, acids and furans were determined by HPLC using an Agilent 1260 series instrument equipped with a refractive index detector and Bio-Rad Aminex HPX-87H column, coupled with a guard column assembly. Product separation was obtained at 60 °C with 4 mM H_2SO_4 as a mobile phase at a flow rate of 0.6 mL/min column temperature of 60 °C. Sample injection volumes of 5 µL were used. Prior to analysis, samples were filtered through 0.45 µm centrifuge filters. The concentrations of glucose, xylose, acetic acid, formic acid, lactic acid, 5-hydroxymethylfurfural and furfural were monitored by a refractive index detector (kept at 35 °C and configured for a 4 s response time) and their concentrations were calculated by integration of peak areas and comparison to a calibration curve made from pure standards.

Aromatics: To quantify aromatics, sample supernatants were collected and filtered through 0.45 µm centrifuge filters before HPLC analysis. The separation of compounds was performed using an Agilent Technologies 1260 infinity series HPLC system equipped with an Eclipse Plus Phenylhexyl column (250 mm length, 4.6 mm diameter, 5 µm particle size; Agilent Technologies, USA) that was maintained at 50 °C, using an injection volume of 5 µL. The mobile phase was composed of 10 mM ammonium acetate in water (solvent A) and 10 mM ammonium acetate in acetonitrile 90% (solvent B), prepared from a stock solution of 100 mM ammonium acetate and 0.7% formic acid in water. The following mobile phase gradient profile was used: 30% B (0 min;

0.5 mL/ min), 80% B (12 min; 0.5 mL/min), 100% B (12.1 min; 0.5 mL/min), 100% B (12.6 min; 1 mL/min), 30% B (12.8 min; 1 mL/min), 30% B (15.6 min; 1 mL/min). Diode array detectors set at 254, 280 and 310 nm wavelengths were used for detection. Concentrations were determined using calibration curves made with peak areas obtained from pure standards.

Alkanolamines: Liquid chromatography (LC) was conducted on a ZIC-pHILIC column (150-mm length, 4.6-mm internal diameter, and 5-µm particle size; Sigma Aldrich, St. Louis, MO, USA) using an Agilent Technologies 1260 HPLC system (Agilent Technologies, Santa Clara, CA, USA). A sample injection volume of 5 µL was used. The sample tray and column compartment were set to ambient temperature and 25°C, respectively. The mobile phase was composed of 10 mM ammonium formate and 0.07% formic acid (Sigma-Aldrich, St. Louis, MO, USA) in 54% acetonitrile. Ethanolamine was separated via isocratic elution at flow rate of 0.8 mL/min. The total LC run time was 8 min. The HPLC system was coupled to an Agilent Technologies 6520 Quadrupole Time-of-Flight Mass Spectrometer (QTOF-MS). Drying and nebulizing gases were set to 11 L/min and 30 lb/in2, respectively, and a drying-gas temperature of 330°C was used throughout. Electrospray ionization was conducted in the positive ion mode with a capillary voltage of 3,500 V. The fragmentor, skimmer, and OCT 1 RF Vpp voltages were set to 100, 65, and 170 V, respectively. The acquisition range was from 55-500 m/z, and the acquisition rate was 0.86 spectra/sec. Reference mass correction was conducted via the phthalic anhydride 149.0239 m/z [F + H] ion (which is a fragment (F) ion from phthalate esters with an empirical formula of C8H4O3). Ethanolamine was detected at 62.06004 m/z via [M + H] ions. The QTOF-MS was tuned with the Agilent ESI-L Low concentration tuning mix in the range of 50-1700 m/z. Data acquisition and processing were conducted via the Agilent MassHunter software package.

Structural Characterization of Biomass Residue Characterization

PXRD: The raw and pretreated biomass were dried and characterized using powder X-ray diffraction (PXRD). The XRD analyses were performed on a Bruker D2 Phaser (Bruker Scientific Instruments, Billerica, MA) and operated at 30 kV and 10 mA using Cu K-alpha: λ =1.54184 Å. 1.0 mm Soller slit input, 3 mm knife edge on sample, 2.5 mm Soller slit in front of silicon strip detector opened to 4.75 degrees. The patterns were collected in the 2θ range from 5 to 60° with a step size of 0.039° and the exposure time of 300 seconds. A reflection–transmission spinner was used as a sample holder and the spinning rate was set at 8 rpm throughout the experiment.

According to previously defined diffractogram, the Bragg angles of peak (110), (1$\bar{1}$0), (020), and (004) belonging to cellulose I are ~ [14.8°, 16.3°, 22.3°, and 34.5°], respectively. The Bragg angle of the amorphous peak is around 19.5 - 20.5°.[38] The crystallinity index was also calculated according to the method of Segal *et.al.*, where the ratio of the height of the 002 peak (I_{002}) and the height of the minimum (I_{AM}) between the 002 and the 101 peaks.[38,64] The peak deconvolution of the resulting diffractogram was also performed using software PeakFit (SeaSolve Software Inc.). Gaussian/Lorentzian functions were applied in curve fitting analysis and iterations were repeated until the maximum F number was obtained. In all cases, the F number was >10,000, which corresponds to a R^2 value > 0.99. Estimation of the content amorphous cellulose in the cellulosic samples was established by using the relative peak areas.

Thermal Gravimetric Analysis (TGA): Thermal analysis was determined conducted using a Mettler Toledo TGA/DSC1 unit (Mettler Toledo, Leicester, UK) under N_2 atmosphere (50 mL/min). Samples between 10-20 mg were placed in alumina crucibles (150 µL) and heated from ambient temperature to 600 °C at a heating rate of 10 °C/min. The data was analyzed using STARe Evaluation software.

FTIR Analyses: FT-IR spectra were acquired using a Bruker VERTEX 70 system (Billerica, MA) within the range of 4000 to 600 cm^{-1}, resolution of 4cm^{-1} and 32 s scan time. The data was analyzed using OPUS (version 8.2) software.

NMR Analysis: The lignin extract recovered after ethanolamine pretreatment was solubilized in DMSO-d6/pyridine and then analyzed by two-dimensional (2D) ^{13}C–^{1}H heteronuclear single quantum coherence (HSQC) nuclear magnetic resonance (NMR). Briefly, the lignin sample (~50 mg) was solubilized in ~600 µL DMSO-d6/pyridine-d5 (2/1 v/v). The samples were sealed and sonicated until homogeneous in a Branson 2510 table-top cleaner Branson Ultrasonic Corporation, Danburt, CT). The temperature of the bath was closely monitored and maintained below 50 °C. After complete solubilization, the samples were transferred into NMR tubes. 2D HSQC spectra were recorded on a Bruker Avance I spectrometer operating at 800 MHz that was equipped with a TXI probe at 298 K. ^{1}H-^{13}C correlations were obtained using the Q_HSQC method of Heikkinen *et. al.*.[65] The ^{1}H and ^{13}C spectral widths were set to 13.3 ppm and 160 ppm respectively, with carrier frequencies set to 5 ppm (^{1}H) and 80 ppm (^{13}C). A total of 256 scans were collected for each of 256 blocks, using a recycle delay of 1 sec. Chemical shifts were referenced to the central

DMSO peak (δC/δH 39.5/2.5 ppm). Assignment of the HSQC spectra is described elsewhere.[44–46] A semiquantitative analysis of the volume integrals of the HSQC correlation peaks was performed using MestReNova (Mestrelab Research S.L.) processing software, version 14.1.2-25024.

Bioconversion

Bioconversion of hydrolysate was performed using *Rhodosporidium toruloides* that was engineered previously to express the bisabolene synthase gene for production of bisabolene from lignocellulosic derived carbon compounds.[49] Routine cultures of the strain were cultivated at 30 °C using yeast peptone dextrose (YPD, BD Difco, USA) prepared using manufacturer's instructions (to achieve working concentrations of 20 g/L glucose as the primary carbon source). Cells were struck onto a YPD agar plate, from which an individual colony was used to inoculate a 2.5 mL YPD culture containing 50 ug/mL nourseothricin (NTC) and 100 ug/mL cefotaxime (CTX). This antibiotic concentration was maintained for all future cultures. The culture was grown overnight with 200 rpm shaking, and diluted 1/100 into 3 cultures: a 2.5 mL YPD culture, and two 2.5 mL cultures with a 1:1 ratio of YPD to replicate hydrolysates 1 and 2 respectively and further supplemented with 5 g/L $(NH_4)_2SO_4$. Cultures were again incubated overnight with 200 rpm shaking, and Optical Densities at 600nm (OD_{600}) were measured using a SpectraMax microplate reader (Molecular Devices, USA).

Each culture was used to inoculate three new 1 mL cultures at an OD_{600} of 0.2 in either YPD, hydrolysate 1, or hydrolysate 2, with hydrolysates again supplemented with 5 g/L $(NH_4)_2SO_4$ and distributed to individual wells in a 48-well transparent bottom FlowerPlates (m2p labs, Germany). Wells were supplemented with 250 uL of dodecane supplemented with 0.13% pentadecane to collect produced bisabolene, and sealed with an AreaSeal breathable film (Excel Scientific, USA). The FlowerPlate was incubated at 30 °C with 975 rpm shaking and 85% humidity in a BioLector microplate microbioreactor (m2p labs, Germany) with biomass concentration measurements conducted every 30 minutes. A blank well for each media was included with no cell inoculation and used to blank measurements to their time zero biomass concentration measurements. Bioconversion was carried out for 94 hours, after which OD_{600} were immediately quantified using the SpectraMax microplate reader. Cultures from each well were subsequently recovered and centrifuged at 8000 rpm for 60 seconds. 20 uL of the supernatant was diluted in 280 uL of water, filtered through 0.45 um centrifuge filters (VWR, USA), and used for subsequent HPLC analysis.

3 uL of the dodecane layer was collected, diluted into 97 uL of pure dodecane, and used to quantify bisabolene titers via gas chromatography-mass spectroscopy (GC-MS)

To quantify bisabolene produced in the flowerplate cultivations, the diluted dodecane overlays obtained at the end of the experiments were analyzed by GC-MS using an Agilent Technologies 6890N system equipped with a 5973-mass selective detector and a DB-5ms column (30 m x 250 μm x 0.25 μm, Agilent Technologies, USA). 1 μl injections with a splitless setting were used on a GC oven program consisting of 100 °C for 0.75 min, followed by a ramp of 20 °C per min until 300 °C, and held 1 min at 300 °C. Injector and MS quadrupole detector temperatures were 250 °C and 150 °C, respectively. The bisabolene concentrations reported here correspond to the concentrations that would be present in the total culture, obtained by dividing the concentrations measured in the dodecane layer by 5 (250 uL dodecane overlay divided by 1250 uL total culture volume). Bisabolene was calculated by integration of the peak area values obtained in selective ion monitoring mode and compared to the areas obtained from a calibration curve made with pure bisabolene.

Techno Economic Analysis

A commercial-scale cellulosic biorefinery with the nameplate capacity of 2000 bone-dry metric tons of biomass sorghum per day was modeled to assess the economic impact of novel ethanolamine pretreatment investigated in this study. Biomass sorghum feedstock is delivered to the biorefinery in the form of bale with moisture content of 20% (wb). The feedstock supply cost was gathered from our recent work.[56] The modeled biorefinery produces either bioethanol or bisabolane and operates 24 h/day and 330 days/year. Bisabolene is catalytically hydrogenated to convert into bisabolane (a jet fuel equivalent fuel molecule).[53] Apart from bioconversion, fuel recovery, and catalytic upgrading stages, both biofuels require similar other production stages, including feedstock supply and handling, biomass deconstruction, wastewater treatment, onsite energy generation (heat and power), and utility (process water and cooling water). Our models capture the impacts of variations in capital and operating parameters while computing material and energy balances as well as capital and operating costs. The process models developed in this study are based on the methods and assumptions discussed in similar prior works for ethanol[58,66] and bisabolene.[53] Here, we updated the biomass deconstruction unit, including pretreatment and enzymatic hydrolysis, based on the processes discussed and results obtained in this work.

Additionally, we updated the bioconversion stage for bisabolene based on the operating conditions and bisabolene yield obtained in this study. The operating conditions and assumptions for the remaining stages were consistent with prior works documented on ethanol[58,66,67] and bisabolane.[53] Briefly, the centrifugation-distillation-decantation system was used to recover bisabolene and then catalytically hydrogenated to bisabolane.[53] Ethanol was recovered using distillation and purified using molecular sieve adsorption.[58] Lignin was separated during the fuel recovery process and routed to the onsite energy generation unit. The lignin fraction of biomass and biogas generated from the unutilized sugar were used to generate process steam and electricity onsite. Natural gas was used as a supplemental energy source, required only for bisabolane because of the energy intensive aerobic bioconversion process.[53]

This study also compares the biomass deconstruction cost with ethanolamine demonstrated in this study to prior studies that used ethanolamine acetate[14] and cholinium lysinate[52] [Ch][Lys] as pretreatment solvents. We developed separate biorefinery models considering operating conditions discussed in this work and prior studies. This only requires updating the biomass deconstruction unit and the remaining stages and operating conditions were the same as ethanolamine. For this comparison, we considered biomass sorghum as a model biomass feedstock and ethanol as a model biofuel, adjusting for difference in sorghum composition relative to the feedstocks used in the prior studies (e.g., the ethanolamine acetate study originally used switchgrass as a feedstock). The prior study on ethanolamine acetate demonstrated glucose and xylose yields of 72% and 56% of the theoretical maximums, respectively, with a biomass loading rate of 40 wt% based on the whole slurry.[14] The biomass loading rate of 40% is the same in this study, but the enzyme loading rate of 20 mg-protein/g-biomass in the prior study is two-fold more than this study. Prior work with cholinium lysinate[52] [Ch][Lys] used biomass sorghum feedstock and an enzyme loading rate of 10 mg-protein/g-biomass (consistent with this study). For comparison, we considered the glucose and xylose yields obtained in the prior work with cholinium lysinate[52] [Ch][Lys] of 80.52% and 61.68%, respectively. The capital and operating costs obtained from the process model were used in a discounted cash flow analysis rate of return analysis to determine the minimum selling price of biofuel at the biorefinery gate and contributions from several biofuel production stages. The minimum selling price was determined based on an internal rate of return of 10%, service life of the facility of 30 years, and income tax rate of 21%.[67] The remaining economic evaluation parameters were consistent with prior NREL analyses.[58,67]

COSMO-RS Calculations

To perform the COSMO-RS calculations, the molecular structures of all the investigated solvents (ethanolamine, 1-amino-2-propanol, 2-(methylamino)ethanol, N,N-dimethylethanolamine, 1,3-diamino-2-propanol, and 2-amino-1,3-propanediol) and lignin are drawn using Avogadro freeware software.[68] In the literature, lignin monomeric or dimeric structures were used to represent the lignin model for COSMO-RS simulations.[69] However, this monomeric and dimeric structures of lignin do not directly represent lignin due to the absence of many different linkages present in lignin. Therefore, herein we built the lignin molecule by joining all the major linkages (such as β-O-4, β-β, 4-O-5, α-O-4, and β-5) present in the native lignin (see figure S1). The geometries of all the molecules were optimized by using the Gaussian09 package at B3LYP theory and 6-311+G(d,p) basis set.[70] Further, the frequency calculations have also been performed to confirm the stable structure and verify the presence of any imaginary frequency if presence. From the frequency calculations, no imaginary frequencies were present after optimization.

After a geometry optimization, the next step is to generate the COSMO files. The COSMO files of investigated molecules were generated using the BVP86/TZVP/DGA1 level of theory and basis set.[71–73] The ideal screening charges on the molecular surface were computed using the same level of theory (BVP86) through the "scrf = COSMORS" keyword.[72,74] Finally, the generated COSMO files were then used as an input in the COSMOtherm (version 19.0.4, COSMOlogic, Leverkusen, Germany) package.[75] BP_TZVP_19 parametrization was used to predict the sigma potentials, viscosity, excess enthalpy, and logarithmic activity coefficients of the isolated and mixture of molecular systems (i.e., lignin-alkanolamines). The details of COSMO-RS calculation in predicting the sigma potential, excess enthalpies, and activity coefficients are provided in the COSMOtherm's user manual.[76]

SUPPLEMENTARY INFORMATION

The COSMO-RS calculated chemical potentials of investigated molecules, viscosity validation, lignin developed predictive model plots, and quantum-based calculated intermolecular geometries are presented in the supplementary information along with this manuscript. Also, additional information is presented on the ANOVA, biomass characterization (PXRD/TGA/FTIR/NMR analyses), bioconversion and technoeconomic analyses.

AUTHOR INFORMATION

Corresponding Authors

* E-mail: *jmgladden@lbl.gov;* jmgladd@sandia.gov (John M. Gladden)

CONFLICTS OF INTEREST

The authors declare the following competing financial interest(s): ECA, BAS, and JMG are named inventors on at least one related patent application. The authors have no other relevant affiliations or financial involvement with any organization or entity with a financial interest in or financial conflict with the subject matter or materials discussed in the manuscript apart from those disclosed.

ACKNOWLEDGEMENTS

This work was part of the DOE Joint BioEnergy Institute (http:// www.jbei.org) supported by the U. S. Department of Energy, Office of Science, Office of Biological and Environmental Research, through contract DE-AC02-05CH11231 between Lawrence Berkeley National Laboratory and the U. S. Department of Energy. The United States Government retains and the publisher, by accepting the article for publication, acknowledges that the United States Government retains a non-exclusive, paid-up, irrevocable, world-wide license to publish or reproduce the published form of this manuscript, or allow others to do so, for United States Government purposes. XRD characterization was conducted with the help of Jakob Dahl and the Alivisatos Group in the College of Chemistry at the University of California, Berkeley. LC-MS Characterization was conducted with the help of Ramu Kakumanu, Ph.D. and Edward E. K. Baidoo Ph.D. of the Functional Genomics Division in the Joint BioEnergy Institute (Lawrence Berkeley National Lab).

BIBLIOGRAPHY

1. J. L. Field, T. L. Richard, E. A. H. Smithwick, H. Cai, M. S. Laser, D. S. LeBauer, S. P. Long, K. Paustian, Z. Qin, J. J. Sheehan, P. Smith, M. Q. Wang, and L. R. Lynd, *Proc. Natl. Acad. Sci. USA*, 2020, **117**, 21968–21977.
2. N. R. Baral, E. R. Sundstrom, L. Das, J. M. Gladden, A. Eudes, J. Mortimer, S. W. Singer, A. Mukhopadhyay, and C. D. Scown, *ACS Sustain. Chem. Eng.*, 2019, **7**, 9062–9079.
3. B. Yang and C. E. Wyman, *Biofuels, Bioprod. Bioref.*, 2008, **2**, 26–40.
4. A. Anukam and J. Berghel, in *Biomass [Working Title]*, IntechOpen, 2021.
5. M. Galbe and O. Wallberg, *Biotechnol Biofuels*, 2019, **12**, 294.
6. D. M. Alonso, S. H. Hakim, S. Zhou, W. Won, O. Hosseinaei, J. Tao, V. Garcia-Negron, A. H. Motagamwala, M. A. Mellmer, K. Huang, C. J. Houtman, N. Labbé, D. P. Harper, C. Maravelias, T. Runge, and J. A. Dumesic, *Sci. Adv.*, 2017, **3**, e1603301.
7. Z. Strassberger, S. Tanase, and G. Rothenberg, *RSC Adv.*, 2014, **4**, 25310–25318.
8. P. Kumar, D. M. Barrett, M. J. Delwiche, and P. Stroeve, *Ind Eng Chem Res*, 2009, **48**, 3713–3729.
9. L. Yao, C. Chen, C. G. Yoo, X. Meng, M. Li, Y. Pu, A. J. Ragauskas, C. Dong, and H. Yang, *ACS Sustain. Chem. Eng.*, 2018, **6**, 14767–14773.
10. J. Kautto, M. J. Realff, A. Ragauskas, and T. Kässi, *BioRes*, 2014, **9**, 6041–6072.
11. Z. Zhang, M. D. Harrison, D. W. Rackemann, W. O. S. Doherty, and I. M. O'Hara, *Green Chem.*, 2016, **18**, 360–381.
12. A. Rodríguez, E. Espinosa, J. Domínguez-Robles, R. Sánchez, I. Bascón, and A. Rosal, in *Pulp and paper processing*, ed. S. N. Kazi, InTech, 2018.
13. F. Cheng, T. Ouyang, J. Sun, T. Jiang, and J. Luo, *BioRes*, 2019, **14**, 486–499.
14. J. Sun, N. V. S. N. M. Konda, R. Parthasarathi, T. Dutta, M. Valiev, F. Xu, B. A. Simmons, and S. Singh, *Green Chem.*, 2017, **19**, 3152–3163.

15. R. M. Dias, F. H. B. Sosa, and M. C. da Costa, *Polym. Bull.*, 2019.

16. N. I. Haykir, E. Bahcegul, N. Bicak, and U. Bakir, *Ind. Crops Prod.*, 2013, **41**, 430–436.

17. I. Anugwom, V. Eta, P. Virtanen, P. Mäki-Arvela, M. Hedenström, M. Hummel, H. Sixta, and J.-P. Mikkola, *ChemSusChem*, 2014, **7**, 1170–1176.

18. Z. Zhao, X. Chen, M. F. Ali, A. A. Abdeltawab, S. M. Yakout, and G. Yu, *Bioresour. Technol.*, 2018, **263**, 325–333.

19. A. Rodríguez, L. Serrano, A. Moral, and L. Jiménez, *Biochem Eng J*, 2008, **42**, 243–247.

20. A. Rodríguez, L. Serrano, A. Moral, A. Pérez, and L. Jiménez, *Bioresour. Technol.*, 2008, **99**, 1743–1749.

21. S. Hedjazi, A. H. Adli, A. J. Latibari, Y. Hamzeh, and M. Ahmadi, 2011.

22. R. Patt and A. Kreipl, 2010.

23. F. Yang and P. Feng, *Appl. Sci.*, 2020, **10**, 8342.

24. D. Yalcin, A. J. Christofferson, C. J. Drummond, and T. L. Greaves, *Phys. Chem. Chem. Phys.*, 2020, **22**, 10995–11011.

25. F. Xu, J. Sun, N. V. S. N. M. Konda, J. Shi, T. Dutta, C. D. Scown, B. A. Simmons, and S. Singh, *Energy Environ. Sci.*, 2016, **9**, 1042–1049.

26. J. Y. Zhu, X. Pan, and R. S. Zalesny, *Appl. Microbiol. Biotechnol.*, 2010, **87**, 847–857.

27. C. W. Edmunds, P. Peralta, S. S. Kelley, V. L. Chiang, R. R. Sharma-Shivappa, M. F. Davis, A. E. Harman-Ware, R. W. Sykes, E. Gjersing, M. W. Cunningham, W. Rottmann, Z. D. Miller, and I. Peszlen, *Cellulose*, 2017, **24**, 1901–1914.

28. T. Dutta, G. Papa, E. Wang, J. Sun, N. G. Isern, J. R. Cort, B. A. Simmons, and S. Singh, *ACS Sustain. Chem. Eng.*, 2018, **6**, 3079–3090.

29. J. Y. Zhu and X. J. Pan, *Bioresour. Technol.*, 2010, **101**, 4992–5002.

30. A. Fernández-Agulló, M. S. Freire, C. Ramírez-López, J. Fernández-Moya, and J. González-Álvarez, *Biomass Conv. Bioref.*, 2020.

31. F. Bertaud, C. Crampon, and E. Badens, *Holzforschung*, 2017.

32.

33. M. Galbe and G. Zacchi, *Adv Biochem Eng Biotechnol*, 2007, **108**, 41–65.

34. S. P. S. Chundawat, G. Bellesia, N. Uppugundla, L. da Costa Sousa, D. Gao, A. M. Cheh, U. P. Agarwal, C. M. Bianchetti, G. N. Phillips, P. Langan, V. Balan, S. Gnanakaran, and B. E. Dale, *J. Am. Chem. Soc.*, 2011, **133**, 11163–11174.

35. T. Cui, J. Li, Z. Yan, M. Yu, and S. Li, *Biotechnol Biofuels*, 2014, **7**, 134.

36. A. Mittal, R. Katahira, M. E. Himmel, and D. K. Johnson, *Biotechnol Biofuels*, 2011, **4**, 41.

37. E.-L. Hult and T. Iversen, *Springer Science and Business Media LLC*, 2003.

38. S. Park, J. O. Baker, M. E. Himmel, P. A. Parilla, and D. K. Johnson, *Biotechnol Biofuels*, 2010, **3**, 10.

39. O. Faix, in *Methods in lignin chemistry*, eds. S. Y. Lin and C. W. Dence, Springer Berlin Heidelberg, Berlin, Heidelberg, 1992, pp. 83–109.

40. D. Y. Corredor, J. M. Salazar, K. L. Hohn, S. Bean, B. Bean, and D. Wang, *Appl. Biochem. Biotechnol.*, 2009, **158**, 164–179.

41. C. F. B. Sene, M. C. McCann, R. H. Wilson, and R. Grinter, *Plant Physiol.*, 1994, **106**, 1623–1631.

42. R. Liu, H. Yu, and Y. Huang, *Cellulose*, 2005, **12**, 25–34.

43. K. K. Pandey, *J. Appl. Polym. Sci.*, 1999, **71**, 1969–1975.

44. W. Li, K. Amos, M. Li, Y. Pu, S. Debolt, A. J. Ragauskas, and J. Shi, *Biotechnol Biofuels*, 2018, **11**, 304.

45. A. Eudes, T. Dutta, K. Deng, N. Jacquet, A. Sinha, V. T. Benites, E. E. K. Baidoo, A. Richel, S. E. Sattler, T. R. Northen, S. Singh, B. A. Simmons, and D. Loqué, *PLoS One*, 2017, **12**, e0178160.

46. H. Kim and J. Ralph, *Org. Biomol. Chem.*, 2010, **8**, 576–591.

47. J.-L. Wen, S.-L. Sun, B.-L. Xue, and R.-C. Sun, *J. Agric. Food Chem.*, 2013, **61**, 635–645.

48. B. B. Hallac, Y. Pu, and A. J. Ragauskas, *Energy Fuels*, 2010, **24**, 2723–2732.

49. J. Yaegashi, J. Kirby, M. Ito, J. Sun, T. Dutta, M. Mirsiaghi, E. R. Sundstrom, A. Rodriguez, E. Baidoo, D. Tanjore, T. Pray, K. Sale, S. Singh, J. D. Keasling, B. A. Simmons, S. W. Singer, J. K. Magnuson, A. P. Arkin, J. M. Skerker, and J. M. Gladden, *Biotechnol Biofuels*, 2017, **10**, 241.

50. E. Sundstrom, J. Yaegashi, J. Yan, F. Masson, G. Papa, A. Rodriguez, M. Mirsiaghi, L. Liang, Q. He, D. Tanjore, T. R. Pray, S. Singh, B. Simmons, N. Sun, J. Magnuson, and J. Gladden, *Green Chem.*, 2018, **20**, 2870–2879.

51. A. Rodriguez, N. Ersig, G. M. Geiselman, K. Seibel, B. A. Simmons, J. K. Magnuson, A. Eudes, and J. M. Gladden, *Bioresour. Technol.*, 2019, **286**, 121365.

52. H. D. Magurudeniya, N. R. Baral, A. Rodriguez, C. D. Scown, J. Dahlberg, D. Putnam, A. George, B. A. Simmons, and J. M. Gladden, *Green Chem.*, 2021, **23**, 3127–3140.

53. N. R. Baral, O. Kavvada, D. Mendez-Perez, A. Mukhopadhyay, T. S. Lee, B. A. Simmons, and C. D. Scown, *Energy Environ. Sci.*, 2019, **12**, 807–824.

54. A. Rodrigues Gurgel da Silva, M. Errico, and B.-G. Rong, *Clean Techn. Environ. Policy*, 2017, **20**, 1–12.

55. C. A. Barcelos, A. M. Oka, J. Yan, L. Das, E. C. Achinivu, H. Magurudeniya, J. Dong, S. Akdemir, N. R. Baral, C. Yan, C. D. Scown, D. Tanjore, N. Sun, B. A. Simmons, J. Gladden, and E. Sundstrom, *ACS Sustain. Chem. Eng.*, 2021.

56. N. R. Baral, J. Dahlberg, D. Putnam, J. C. Mortimer, and C. D. Scown, *ACS Sustain. Chem. Eng.*, 2020, **8**, 15855–15864.

57. M. J. Dunlop, Z. Y. Dossani, H. L. Szmidt, H. C. Chu, T. S. Lee, J. D. Keasling, M. Z. Hadi, and A. Mukhopadhyay, *Mol. Syst. Biol.*, 2011, **7**, 487.

58. D. Humbird, R. Davis, L. Tao, C. Kinchin, D. Hsu, A. Aden, P. Schoen, J. Lukas, B. Olthof, M. Worley, D. Sexton, and D. Dudgeon, *Process Design and Economics for Biochemical Conversion of Lignocellulosic Biomass to Ethanol: Dilute-Acid Pretreatment and Enzymatic Hydrolysis of Corn Stover*, National Renewable Energy Laboratory (NREL), Golden, CO (United States), 2011.

59. J. Kirby, G. M. Geiselman, J. Yaegashi, J. Kim, X. Zhuang, M. B. Tran-Gyamfi, J.-P. Prahl, E. R. Sundstrom, Y. Gao, N. Munoz, K. E. Burnum-Johnson, V. T. Benites, E. E. K. Baidoo, A. Fuhrmann, K. Seibel, B.-J. M. Webb-Robertson, J. Zucker, C. D. Nicora, D. Tanjore, J. K. Magnuson, J. M. Skerker, and J. M. Gladden, *Biotechnol Biofuels*, 2021, **14**, 101.

60. F. Xu, J. Sun, M. Wehrs, K. H. Kim, S. S. Rau, A. M. Chan, B. A. Simmons, A. Mukhopadhyay, and S. Singh, *ACS Sustain. Chem. Eng.*, 2018, **6**, 8914–8919.

61. Sluiter, Hames, Ruiz, Scarlata, Sluiter, and Templeton, *NREL*, 2008, **TP-510-42618**.

62. S. D. Mansfield, H. Kim, F. Lu, and J. Ralph, *Nat. Protoc.*, 2012, **7**, 1579–1589.

63. S. Liu, L. Das, D. N. Blauch, C. Veronee, C. Dou, J. Gladden, N. Sun, and A. M. Socha, *Green Chem.*, 2020.

64. L. Segal, J. J. Creely, A. E. Martin, and C. M. Conrad, *Textile Research Journal*, 1959, **29**, 786–794.

65. S. Heikkinen, M. M. Toikka, P. T. Karhunen, and I. A. Kilpeläinen, *J. Am. Chem. Soc.*, 2003, **125**, 4362–4367.

66. M. Yang, N. R. Baral, B. A. Simmons, J. C. Mortimer, P. M. Shih, and C. D. Scown, *Proc. Natl. Acad. Sci. USA*, 2020, **117**, 8639–8648.

67. R. E. Davis, N. J. Grundl, L. Tao, M. J. Biddy, E. C. Tan, G. T. Beckham, D. Humbird, D. N. Thompson, and M. S. Roni, *Process design and economics for the conversion of lignocellulosic biomass to hydrocarbon fuels and coproducts: 2018 biochemical design case update; biochemical*

deconstruction and conversion of biomass to fuels and products via integrated biorefinery pathways, National Renewable Energy Laboratory (NREL), Golden, CO (United States), 2018.

68. M. D. Hanwell, D. E. Curtis, D. C. Lonie, T. Vandermeersch, E. Zurek, and G. R. Hutchison, *J. Cheminform.*, 2012, **4**, 17.

69. C. Balaji, T. Banerjee, and V. V. Goud, *J. Solution Chem.*, 2012, **41**, 1610–1630.

70. M. Mohan, C. Balaji, V. V. Goud, and T. Banerjee, *J. Solution Chem.*, 2015, **44**, 538–557.

71. M. Mohan, T. Banerjee, and V. V. Goud, *Journal of Chemical & Engineering Data*, 2016, **61**, 2923–2932.

72. M. Mohan, V. V. Goud, and T. Banerjee, *Fluid Phase Equilib.*, 2015, **395**, 33–43.

73. M. Mohan, P. Viswanath, T. Banerjee, and V. V. Goud, *Mol. Phys.*, 2018, **116**, 1–21.

74. M. Mohan, T. Banerjee, and V. V. Goud, *Can. J. Chem. Eng.*, 2018.

75. F. Eckert and A. Klamt, *AIChE Journal*, 2002, **48**, 369–385.

76. F. Eckert and A. Klamt, *COSMOtherm, version C3.0 release 19.0.1*, COSMOlogic GmbH & Co KG, Leverkusen, Germany, 2019, C3.0 release 19.0.1.